DUPLICATE ALSO (266)

Long-Range Forecasting and Climate Research

The Climate of the World

5. Ocean-Atmosphere Interaction

by

D. E. Parker and C. K. Folland

LRFC 24

July 1988

ORGS UKMO L

National Meteorological Library
FitzRoy Road, Exeter, Devon. EX1 3PB

FHIB

DUPLICATE ALSO

METEOROLOGICAL OFFICE
15 AUG 1988
LIBRARY

LS/M013

LONG RANGE FORECASTING AND CLIMATE RESEARCH MEMORANDUM NO 24
(LRFC 24)

THE CLIMATE OF THE WORLD

5. OCEAN-ATMOSPHERE INTERACTION

by

D E PARKER AND C K FOLLAND

NOTES FOR AN ADVANCED LECTURE FOR THE SCIENTIFIC OFFICERS' COURSE, METEOROLOGICAL OFFICE, 1988

Met O 13 (Synoptic Climatology Branch)
Meteorological Office
London Road
Bracknell
Berkshire
RG2 2SZ

July 1988

Note: This paper has not been published. Permission to quote from it should be obtained from the Assistant Director (Synoptic Climatology), Meteorological Office.

LONDON, METEOROLOGICAL OFFICE.
Long-Range Forecasting and Climate Research
Memorandum No.24

The climate of the world.
5. Ocean-atmosphere interaction.

00150988 FH1B

This Memorandum is the third in a series of seven on:

THE CLIMATE OF THE WORLD

BY

C K Folland and D E Parker

Based on ten Advanced Lectures for the Scientific Officers' Course, 1988, and one Advanced Lecture delivered by D J Carson in March 1982.

INDEX TO SERIES

LRFC 22	1.	INTRODUCTION TO WORLD CLIMATE
	2.	DESCRIPTION OF WORLD CLIMATE (Advanced Lectures 1 and 2). C K Folland and D E Parker
LRFC 23	3.	CLIMATIC FORCING AND FEEDBACK PROCESSES. I. FORCING FROM ABOVE
	4.	CLIMATIC FORCING AND FEEDBACK PROCESSES. II. INTERACTIONS WITH THE LAND SURFACE (Advanced Lectures 3 and 4). C K Folland and D E Parker
LRFC 24	5.	OCEAN-ATMOSPHERE INTERACTION (Advanced Lecture 5). D E Parker and C K Folland
LRFC 25	6.	THE EL NINO/SOUTHERN OSCILLATION, THE QUASI-BIENNIAL OSCILLATION, AND THE 30-60 DAY VARIATIONS. (Advanced Lecture 6). C K Folland and D E Parker
LRFC 26	7.	A REVIEW OF PALAEOCLIMATE FROM THE EARLY EARTH TO THE PLEISTOCENE ICE AGES
	8.	CLIMATE FROM THE LATE GLACIAL TO THE "LITTLE ICE AGE" (Advanced Lectures 7 and 8). C K Folland and D E Parker
LRFC 27	9	CLIMATIC CHANGE IN THE INSTRUMENTAL PERIOD (Advanced Lecture 9). D E Parker and C K Folland
LRFC 28	10	CARBON DIOXIDE AND OTHER GREENHOUSE GASES, AND CLIMATIC VARIATION (WITH APPENDIX ON SIMPLE CLIMATE MODELS). (Advanced Lecture 10 plus an Advanced Lecture delivered by D J Carson in March 1982). D E Parker, C K Folland and D J Carson.

ADVANCED LECTURE NO 5

OCEAN-ATMOSPHERE INTERACTION

D E PARKER AND C K FOLLAND

MET O 13

SUMMARY

It is well-known that differences in temperature between land and sea play an important role in shaping the observed seasonal variations in atmospheric circulation. We demonstrate from theoretical, empirical and numerical-modelling results that variations in sea surface temperature on several time-scales additional to the climatologically averaged seasonal variations are an important influence on climatic variability. Examples are given both for the midlatitudes and for the tropics. Recent research into the causes and predictability of the droughts in sub-Saharan Africa indicates that modulation of the tropical atmospheric circulation by worldwide sea surface temperature anomalies has a greater influence on sub-Saharan rainfall than do regional anomalies of soil moisture. Furthermore, these atmospheric circulation changes may reinforce the decadal and longer time-scale variations in sea surface temperature, by modulating surface ocean currents.

5.1 INTRODUCTION

In many parts of the world, sea surface temperature (SST) varies substantially through the seasons, but the greater seasonal cycle of air temperature over land (Fig 5.1) results in seasonally varying differences in temperature between land and sea, which play an important role in shaping the observed seasonal variations in atmospheric circulation.

At first sight, however, it is not self-evident that variations in SST that occur in addition to the mean seasonal variations are an important influence on climatic variability. In this lecture, therefore, we

demonstrate the importance of regional and global-scale nonseasonal variations or "anomalies" of SST in relation to climatic variations on seasonal, interannual and decadal time-scales. We leave century time-scale variations to Lecture 9, and geological time-scale variations to Lectures 7 and 8. Also we leave discussion of the El Nino-Southern Oscillation to Lecture 6, and, after discussions of general principles and of the effects of extratropical and tropical SST anomalies on climatic variability, we concentrate on recently-discovered links between worldwide SST anomalies and rainfall in sub-Saharan Africa.

5.2 SST ANOMALIES

5.2.1 The importance of SST anomalies

The following discussion is based on considerations raised by Sawyer (1965). Suppose that an SST anomaly is suddenly "switched on". Before the atmosphere has begun to readjust there will be anomalous heat transfer ΔQ into the ocean consisting of anomalous sensible and latent heating ΔH and ΔE such that

$$\Delta Q = \Delta H + \Delta E$$

$$= 2.4U\Delta\ (T_a - T_s) + 3.7U\Delta\ (e_a - e_s)\ Wm^{-2} \qquad (5.1)$$

where $\Delta\ (T_a - T_s)$ is the change in the difference between the air temperature T_a and the sea surface temperature T_s; $\Delta\ (e_a - e_s)$ is the change in the difference between the vapour pressure e_a of the air (mb) and the saturation vapour pressure e_s at temperature T_s; U is the wind speed in ms^{-1}; and the constants are empirically determined. Suppose that it is midlatitude winter with U = 10 ms^{-1} and T_s = 15°C. Then if T_s is raised by 1°C, which is a typical magnitude for an SST anomaly (Section 5.2.2), but U, T_a and e_a are held constant, ΔQ is about - 65 Wm^{-2} representing anomalous heat transfer of this magnitude into the atmosphere. This quantity is over 25% of the annual mean absorption of solar energy by the Earth at midlatitudes, which is about 200 Wm^{-2} (Gill (1982)). In practice this calculation exaggerates ΔQ because e_a and T_a are held fixed, but it

suggests that, if equilibrium is to be restored, significant changes of atmospheric circulation are needed, especially if the SST anomaly is in regions of strong winds and of high T_s so that $\frac{de_s}{dT_s}$ is large from the Clausius-Clapeyron equation. In summer, when typical wind speeds are about half their winter values, the anomalous heat transfer for a given magnitude of SST anomaly would be rather more than half its winter value because $\frac{de_s}{dT_s}$ would be greater. In the warmest parts of the oceanic tropics with T_s = 29.5°C and U = 5 ms^{-1}, ΔQ would be about -55 Wm^{-2} if an SST anomaly of 1°C were suddenly generated. This anomalous transfer is comparable with the average net heat transfer (including radiation) at the ocean surface in tropical regions (Fig 5.2), and is nearly 20% of the annual mean abosrption of solar energy by the Earth in the tropics (300 Wm^{-2}, Gill (1982)).

An order-of-magnitude estimate of the impact of a regional SST anomaly on the dynamics of the overlying atmosphere may be made by considering the effects of a regional increase ΔT_a of air temperature throughout the troposphere, taken as the 1000 mb to 200 mb layer, with no change in temperature outside the region. If there is no immediate dynamically-induced response from the surrounding atmosphere other than to accept an outflow at higher levels of excess warm air from the heated region, the density of the heated layer will fall by approximately $\frac{\Delta T_a}{T_a}$ and the surface pressure by 0.8 $\frac{\Delta T_a}{T_a} P_s$, where P_s is the initial surface pressure and the factor 0.8 arises because the top 20% of the atmosphere is assumed not to be heated. If P_s = 1000 mb, T_a = 270°K and ΔT_a = 1°C, then the surface pressure will fall by about 3 mb. In practice, an SST anomaly ΔT_s is likely to result in an air temperature anomaly $\Delta T_a \simeq \Delta T_s$ in the lower troposphere but $\Delta T_a > \Delta T_s$ in the upper troposphere because of enhanced release of latent heat, especially in the tropics.

A change of surface pressure of 3 mb is an order of magnitude smaller than the typical changes associated with midlatitude synoptic systems: thus, a typical SST anomaly of order 1°C appears to be insufficient to play a leading role in the development of an individual system. However, monthly averages of surface pressure in midlatitudes have standard deviations of the order of 5 mb in winter (Parker (1982)) and 3 mb in summer, so persistent SST anomalies on the same space scale (several thousand km) as typical anomalies of surface pressure may be important influences on monthly and especially seasonal mean conditions in midlatitudes. In the tropics, the largest surface pressure anomalies on seasonal time-scales are associated with the El Nino-Southern Oscillation (ENSO), in which SST anomalies of several degrees C covering much of the eastern and central tropical Pacific are a key feature (Lecture 6). The influence of other observed tropical SST anomalies on a variety of space and time scales is also expected to be significant in view of the above computations, since these anomalies are often of order 1°C, and since pressure changes of a few millibars entail substantial changes in flow regimes at low latitudes.

5.2.2 The characteristics of SST anomalies

Figs 5.3A and B show the interannual standard deviations of January and July SST as given by Bottomley et al (1988) for the period 1951-80. Areas of high interannual variability include the tropical central and eastern Pacific, the central North Pacific, and the Kuroshio and Gulf Stream regions. Figs 5.3 C and D show one-month lag correlations of SST anomalies between January and February and July and August, respectively. Persistence is greatest in the extratropical North Atlantic, and, except from January to April (Bottomley et al (1988)) in the eastern tropical Pacific. The midlatitude North Pacific also sometimes exhibits persistent SST anomalies, as do parts of the tropical central Pacific, and the tropical Atlantic. Figs 5.3 A to D suggest that the magnitude, spatial scale and persistence of typical SST anomalies in many parts of the world are sufficient to have the significant effects on the atmosphere suggested by the considerations of Sawyer and of Section 5.2.1 above.

Figs 5.4 A, B, C characterise major global patterns of SST anomalies (SSTA) by showing the first three covariance eigenvectors of variation of worldwide fields of SSTA. The eigenvectors were computed from a matrix of seasonal SSTA on a worldwide 10° latitude x longitude grid for the period 1901 to 1980. Missing data in the matrix had first been replaced by interpolated values derived by a combination of polynomial interpolation in time and linear interpolation spacewise. Data for before 1942 had been adjusted to compensate for the use of uninsulated buckets (Bottomley et al (1988)). The first eigenvector (Fig 5.4A) is of the same sign almost everywhere, accounts for 10.9% of the total variance, and represents worldwide long-term trends of SST (Lecture 9). The second eigenvector (Fig 5.4B) represents the signature of El Nino (Lecture 6) and accounts for 7.7% of the total variance. The third eigenvector (Fig 5.4C), which accounts for 3.9% of the total variance, represents a basically interhemispheric contrast of SSTA, but with the northern Indian Ocean and a few other parts of the northern tropics in phase with the Southern Hemisphere, and with weak SSTA in the S Pacific. This eigenvector has been shown to be strongly related to sub-Saharan rainfall (Section 5.4 below).

Corresponding eigenvectors were also computed using SSTA for particular seasons only (eg northern winter = December to February), again for 1901-80. For all 4 seasons, the first two eigenvectors were very similar to Figs 5.4A and B, demonstrating the computational stability of the eigenvectors and their independence of the annual cycle. For northern spring and autumn the third eigenvector was similar to Fig 5.4C, but for northern summer the features of Fig 5.4C were split between the fourth and fifth eigenvectors, and for northern winter between the third and fourth eigenvectors (Folland and Colman (1988)). The pattern in Fig 5.4C is clearly a natural mode of variability in each individual season.

5.3 GENERAL EVIDENCE FOR THE EFFECTS OF SST ANOMALIES

5.3.1 Effects of extratropical SST anomalies on atmospheric circulation

Smagorinsky (1953) carried out the first physically realistic analysis, using a baroclinic model, of the perturbations to an extratropical zonally symmetric wind flow caused by imposed large-scale diabatic heating that varied with longitude. Fig 5.5 is representative of his results. Smagorinsky defined a sinusoidal heating function such that the maximum diabatic heating, Q_{max}, was 209 Wm^{-2} relative to the minimum heating, Q_{min}. The wavelength of the heating function was 160°, and for the results shown in Fig 5.5 the maximum heating is placed at 40° relative longitude and the minimum heating at -40°. Smagorinsky designed the wavelength of this heating variation to correspond roughly with the variation in surface heating in winter due to the distribution of land and sea in the N American sector. He showed (which can be deduced from Fig 5.5) that the Iceland low at the surface should be placed about 20-30° longitude east of the 500 mb Canadian trough in the winter. In Fig 5.5, D is the meridional wavelength of the heating, and h is the height of maximum heating, which includes the effects of latent heat release: for our purpose D = 35° is quite appropriate (Fig 5.5 (A), (B)). This value corresponds to an appreciable positive (or negative) heating anomaly that occupies at least 10° of latitude. Fig 5.5A suggests that the maximum PMSL response would be of magnitude 2 mb/25 Wm^{-2} of forcing and the maximum 500 mb height response would be about 1 dm/25 Wm^{-2}: Fig 5.5B, for which the height of maximum heating is greater and possibly more realistic, suggests a somewhat smaller response.

We can attempt to apply these ideas to work carried out by Ratcliffe and Murray (1970) (RM), who showed from observations an association between Northern Hemisphere mean sea level pressure (PMSL) anomalies and SST anomalies (SSTA) in the previous month in the "Ratcliffe region" south east of Newfoundland. Fig 5.6 shows the SSTA patterns, in a generalised way, and Fig 5.7 (A), (B) the response of the PMSL to warm and cool anomalies; their wavelike pattern is reminiscent of Smagorinsky's results.

Concentrating on the February PMSL response, the magnitude of the PMSL anomalies is roughly the same for both cool and warm SSTA, but the patterns are not the inverse of each other, suggesting non-linearity in the response of PMSL to SSTA, and that Smagorinsky's model is not wholely appropriate for the shapes and sizes of the areas of SST anomalies in Fig 5.6. In February, U is approximately 11 m sec^{-1} south east of Newfoundland and T_s is approximately 10°C, so a mean maximum SSTA of 1.5°C might give a maximum heating anomaly of nearly 90 Wm^{-2}. Fig 5.5B suggests a PMSL response of about 5 mb downstream of this SSTA value. This response is quite similar to RM's values. In summer the general shape of the PMSL anomaly pattern is similar but anomalies are rather less than half those observed in February. This seems reasonable as on average U will be about half the value observed in February, but is a little less than might have been expected from Section 5.2.1 in view of the greater value of $\frac{de_s}{dT_s}$ in summer.

RM's results have been tested in winter by Palmer and Sun (1985) (PS) using the Meteorological Office 5-level AGCM supported by an observational analysis employing better SST data than were available to RM. The modelling study used warm and cold SSTA whose maximum magnitude just exceeded 3°C, ie double that used by RM; these anomalies are still realistic and correspond to the maximum observed anomalies. The model was initialised from real November atmospheric data and used winter radiation. Four pairs of anomaly (warm SSTA) and control (cold SSTA) runs were made. December climatological mean SST was used away from the anomaly. The differences in model 1000 mb height and 500 mb height between warm and cold cases are shown in Figs 5.8 A and B; in each diagram the difference is averaged over the four pairs of integrations for model days 21-50. The patterns are reminiscent of those of RM but the high and low centres, which are statistically significant, are further apart. The maximum response of about 1.5 mb/°C is weaker than RMs results, possibly because the area of $|SSTA| > 2°C$ was only about 8° latitude x15° longitude. Other details of the model response are given in the paper including the anomalous tracks of depressions. PS believe that the anomalous advection of low-level warm, humid air into the SST anomaly area from the south is an important component of the atmospheric response, which also tends to maintain the SST

anomaly. This provides an important difference between the Smagorinsky model and the probable atmospheric response over the "Ratcliffe" area. However, PS found, by using halved SSTA, that their model's response was approximately linear.

The observational study consisted of a calculation of PMSL and 500 mb height differences between winter months (Nov-Feb) having a warm SSTA (> 0.8°C) and those having a cool SSTA (< -0.8°C) in the region 40°-50°N, 40°-60°W. The epoch 1951-80 was studied first and gave similar results to those of the AGCM though with a slightly shorter wavelength between high and low centres at both levels, when monthly mean SSTA, PMSL and 500 mb height were calculated for the same month. The analysis was repeated for 1901-30 and gave similar results. Fig 5.9 is an example of the results for 1951-80. However, when PMSL was allowed to lag one month behind SSTA the relationships did not hold up well nor did they agree well with those of RM: weak low pressure anomalies were indicated stretching across the Atlantic when data for months following warm SSTA were subtracted from those following cold SSTA. PS pointed out that RM's results for December to January were not statistically significant, and that SSTA southeast of Newfoundland are not persistent at that season. On the other hand, PS found that the relationships were strong (and of the same form as for zero lag) when SSTA was allowed to lag one month behing PMSL, and they therefore suggested that the SSTA develop in response to anomalous atmospheric forcing.

Rowntree (1984) has summarised a number of AGCM experiments carried out in the Atlantic and Pacific on mid-latitude SSTA; Fig 5.10 shows his summary diagramatically; the overall conclusions are surprisingly consistent and broadly in harmony with the ideas of Smagorinsky, though in reality, as hinted above, the relative importance of different physical effects in the atmosphere may vary considerably.

5.3.2 Effects of tropical SST anomalies on atmospheric circulation

Because the Coriolis parameter is small near the equator, the nature of atmospheric forcing by tropical SSTA differs from that by extratropical SSTA. Anomalous tropical heating gives rise to mainly colocated anomalous vertical atmospheric motion, and thus the most direct results of forcing by positive tropical SSTA are local falls of pressure in the lower troposphere and the creation of anomalous anticyclonic vorticity in the upper troposphere. An SSTA centred on or very near the equator forces a pair of low-level low pressure anomalies, one on each side of the equator near the maximum SSTA, with upper-level anticyclonic anomalies overlying them (eg Palmer and Mansfield (1986 a, b)). Simmons (1982) used a relatively simple baroclinic model to show that the anomalous atmospheric vorticity forcing may give rise to a Rossby wave-like response in the extratropics in association with the stimulation of barotropic instability in the upper flow. The atmospheric response in the northern winter was largest in his model when the vorticity forcing in the tropics was placed in specific longitudes and the prescribed climatological mean upper flow included the mean troughs and ridges. The longitudinally varying response did not occur for a prescribed zonally averaged mean flow. Simmons suggested that the effects of tropical vorticity forcing propagate into mid latitudes more easily when the forcing is overlain by upper westerly winds. Upper-tropospheric anticyclonic vorticity responses may be amplified when they coincide with a climatological upper ridge as in the north-east Pacific in winter. Fig 5.11 shows a few of Simmons' results at 500 mb, using a prescribed mean flow defined by a January mean 500 mb height climatology, and with vorticity forcing at 135°E in different tropical latitudes:SST forcing was not explicitly used. Fig 5.11 shows that the strongest extratropical response that Simmons found was for forcing centred at 15°N, 135°E. Note that the 500 mb height response is quite large near the UK in the model.

Palmer and Mansfield (1986b) used the Meteorological Office 11-layer AGCM to explore the impact of tropical W Pacific SSTA on the atmospheric circulation in northern winter. They found that an anomaly

with a maximum of 1.5°C centred on the equator in the tropical W Pacific (see Fig 5.12 A) produced a strong wave-like response in the upper troposphere (Fig 5.12B). The response was statistically significant and was qualitatively similar to that of Simmons. Palmer (1985) argued that the atmospheric response to tropical vorticity forcing may be non-linear; vorticity forcing from positive SSTA mainly results from the increased release of latent heat which would be expected to increase non-linearly with increasing SSTA. Similarly it might be expected that a negative SSTA of given magnitude would produce a smaller vorticity forcing and atmospheric response than a positive SSTA of the same magnitude. Palmer, however, found in his model with negative SSTA a similar magnitude of atmospheric response, though of opposite sign, and gave a straightforward dynamical explanation: the relative vorticity tends to cancel (amplify) the planetary vorticity when the SSTA is positive (negative). However it remains to be seen to what extent such results depend on the AGCM used. Also, extratropical responses to some tropical SSTA may be more barotropically stable than those to other tropical SSTA, and, as a result, less variable and more statistically significant (Palmer (1988)). A contributory reason for the very strong atmospheric response to SSTA over the tropical W Pacific is that a given SSTA produces a larger anomaly of latent heating there than elsewhere because the saturation vapour pressure of ocean water changes faster as temperature changes in the very warm W Pacific water. Typical tropical W Pacific SST's exceed 29°C; occasionally SST exceeds 31°C near the location of the maximum tropical W Pacific SST anomaly used by Palmer and Mansfield (1986).

Fig 5.13 (from Simmons (1982)) shows the response of a steady state linear model to an isolated positive heating anomaly centred on the equator. To the west of the heating maximum, the low level winds tend to be westerly and the upper level winds easterly, a similar situation to that in the real atmosphere west of the diabatic heating maximum in the SE Asian monsoon/W Pacific region in northern summer (see Lecture 2). To the east of the heating maximum, the model winds are reversed: ie the upper winds are westerly and the lower winds easterly. Sinking motion should occur over the well-defined SST minimum near the equatorial S American coast and connect the mean upper westerly to the mean lower easterly flows that exist

to the east of the W Pacific SST maximum. The closed circulation that results is like the Walker circulation discussed in Lecture 2: the mechanism underlying Fig 5.13 probably explains an appreciable part of the Pacific Walker circulation and, perhaps, similar circulations near the equator in other longitudes.

Rowntree (1976) carried out experiments using the Meteorological Office 5-level AGCM which indicated that north of a positive SST anomaly placed in the tropical NE Atlantic in winter a surface low was formed, with an upper-tropospheric high almost over the SST anomaly. North of the low, in fact well into upper middle latitudes, a high anomaly was found. Fig 5.14 shows the model response for selected experiments by comparison with control integrations. The SST anomaly was based on that observed at the beginning of the very cold European winter of 1962-3 but it remains unclear to what extent Rowntree's results "explain" that winter. The differences between Figs 5.14B and C arise because of small changes in model formulation and indicate the sensitivity of the results to such small changes. This is clearly not enough to change the nature of the response in a fundamental way but Figs 5.14B and C show that caution is needed in interpreting the results of model integrations. Statistical significance of model-generated fields needs to be assessed, by Monte Carlo sampling, which may be computationally expensive, or by other techniques described by Livezey and Chen (1983).

Hastenrath (1984) carried out observational studies of tropical Atlantic SSTA and atmospheric circulation anomalies in relation to precipitation in the drought-prone Brazilian Nordeste. Positive SSTA in the tropical South Atlantic and negative SSTA in the tropical North Atlantic were associated with enhanced rainfall in the Nordeste. At the same time, the intertropical convergence zone was displaced southwards and therefore affected the Nordeste to a greater extent. Inverse anomalies were associated with drought in the Nordeste. Hastenrath et al (1984) extended this work by making skilful hindcasts of Nordeste rainfall on the basis of indices of SSTA and atmospheric circulation in the tropical Atlantic region in months prior to the Nordeste's March to May rainy season. Subsequently Ward et al (1988) developed a method of predicting

Nordeste rainfall using only the coefficients of regional eigenvectors of SSTA. One of their eigenvectors corresponded to Hastenrath's North versus South Atlantic SSTA contrast, and another represented El Nino. Skilful predictions were issued for 1987 and 1988.

Tropical SSTA have also been used in the prediction of the Indian Monsoon. In a statistical study, Hastenrath (1987) found that SSTA in the Arabian Sea had predictive value for Indian Monsoon rainfall, and Kershaw (1988) used an atmospheric general circulation model to simulate the effect of a positive SSTA in the eastern Arabian Sea on the onset of the 1979 Indian Monsoon. The SSTA (Fig 5.15A) was appropriate to early June 1979. Beginning with real atmospheric conditions for 11 June 1979, the control integration with climatological SST maintained low-latitude westerlies in the lower troposphere through to 19 June (Fig 5.15B) whereas the anomaly integration produced a lower-tropospheric vortex slightly northwest of the SSTA (Fig 5.15C) and was in generally better agreement with observation (Fig 5.15D), though the strong flow covered too large an area, the centre of the vortex was too far southeast, and the orientation of the strong flow was westerly instead of southwesterly. At 200 mb the anomaly experiment was slightly superior in that it predicted a stronger easterly jet than did the control. The anomaly experiment predicted more precipitation over and to the northwest of the SSTA, with differences exceeding 40 mm per day. Kershaw used diagnostic information from the integrations, as well as a linear model, to elucidate the feedbacks taking place in the model (Fig 5.15E). However the SSTA was held fixed in the model, so the representation of ocean-atmosphere interaction was not complete. In reality, the SSTA would probably have diminished as a result of the increased windiness and cloud cover. This may explain the excessive area of strong flow (ie excessive total kinetic energy) in the lower troposphere in the anomaly experiment (Fig 5.15C: compare with Fig 5.15D).

5.4 SST ANOMALIES AND RAINFALL IN SUB-SAHARAN AFRICA

5.4.1 Introduction

The drought in sub-Saharan Africa has now persisted, with only partial intermissions, for 20 years (Fig 5.16). Folland et al (1986) observed that the decline in Sahel rainfall between the 1950's and the 1970's was accompanied by a warming of the ocean surface in the Southern Hemisphere and northern Indian Ocean (SHNI) and a cooling of the ocean surface in the rest of the Northern Hemisphere (RNH). Since the late 1970's the oceans of both hemispheres have warmed slightly and the difference (SHNI minus RNH) has changed little. Fig 5.17, from Parker and Folland (1988), shows that SSTA differences between 1951-1960 (Sahel wet) and 1971-87 (Sahel dry) exceeded 1°C in some areas. For 1901-84, the correlation between annual Sahel rainfall and the approximately simultaneous (July to September) values of (SHNI minus RNH) was - 0.62 (Folland et al (1984)). Folland et al constructed a difference field between the average July to September SSTA for the very dry years 1972-3, 1982-4 and that for the very wet years 1950, 1952-4, 1958 (Fig 5.18). They then computed the covariance C_i between each year's global field of July to September SSTA field and Fig 5.18, after subtracting the global average SSTA from each field. The correlation between C_i and annual Sahel rainfall was -0.72 for 1901-84. Furthermore, it was -0.85 for 1946-84 and -0.43 for 1901-39. These results suggested that, despite enhancement of the correlations by data-dependence and reduction of significance by lag autocorrelation, the relationship was very strong for the period after 1946 when the prominent fluctuations in Sahel rainfall were interdecadal (Fig 5.16), and still significant for the period 1901-39 which was dominated by interannual variability (Fig 5.16). A parallel exercise using a field corresponding to Fig 5.18 but based on years before 1940 also yielded statistically significant results. The field was similar to Figure 5.18 but with weaker SSTA in the Southern Hemisphere and no major positive SSTA in the East Tropical Pacific. Folland et al (1986) confirmed their findings by applying the SSTA field in Fig 5.18 to the anomaly integration of an atmospheric general circulation model run in perpetual July mode. The

anomaly integration produced a substantially drier Sahel than the control run with climatological SST. The mechanism for reduction of the rainfall in the model appeared to be mainly a reduction in moisture flux covergence, as a result of changes of atmospheric circulation. There was also reduced upper-tropospheric divergence over the Sahel. The modelling experiments were extended by Palmer (1986) who applied the Atlantic, Pacific and Indian Ocean portions of Fig 5.18 separately in a series of anomaly integrations. Over the western Sahel, the Atlantic and Pacific SSTA had a comparable effect in reducing the model's rainfall: over the eastern Sahel, the Indian Ocean had the dominant role.

5.4.2 Confirming the relationships

The pattern in Fig 5.18 has the disadvantage of being based on a small sample of years, and therefore in subsequent studies eigenvector patterns based on the entire 1901-80 data set, rather than composites, have been used to elucidate relationships between SSTA and Sahel rainfall. Comparison of Fig 5.18 with Fig 5.17 suggests that the warm East Tropical Pacific is not a major part of the true Sahel drought signature in SSTA, and that its occurrence in Fig 5.18 is a fortuitous result of the coincidence between the 1982-3 El Nino and very dry conditions in the Sahel. This conclusion is supported by the correlations of only about -0.2 between Sahel rainfall and the simultaneous coefficient of the second worldwide SSTA covariance eigenvector (Fig 5.4B) found by Parker et al (1988). On the other hand, the correlations with the simultaneous coefficient of the third eigenvector (Fig 5.4C) were -0.58, -0.50 and -0.71 for 1901-87, 1901-45, and 1946-85, and both interdecadal and interannual fluctuations contributed to this relationship (Fig 5.19). Note the similarity between the third eigenvector and the recent interdecadal changes in SST shown in Fig 5.17: note also that (SHNI minus RNH) is an approximate measure of the coefficient of the third eigenvector. A smaller part of the SSTA-Sahel rainfall relationship is, however, described by the sixth worldwide eigenvector of SSTA, which mainly represents a contrast between North and South Atlantic SSTA, especially in the Benguela current region, but with the Indian Ocean in phase with the South Atlantic and much of the Pacific Ocean in phase with the North Atlantic (Fig 5.20). The

simultaneous correlation with Sahel rainfall was 0.44 for 1901-86, but the relationship of Sahel rainfall with the sixth eigenvector appears only to have applied during periods when variations have been predominantly interdecadal: see the correlations marked on Fig 5.21, which show that a warm South Atlantic and cold North Atlantic in association with the sixth eigenvector were associated with Sahel drought from 1940 onwards and for a short period at the beginning of the century, but not in the intervening interval. This observation is in accord with the results of Lough (1986), who found that significant relationships established for 1948-72 between Sahel rainfall and a tropical Atlantic SSTA pattern quite similar to the sixth eigenvector did not apply in 1911-39.

A major implication of these results is that Sahel rainfall is related to intrinsic modes of worldwide variability of SSTA. This conclusion could not be drawn from the composite presented in Fig 5.18 or from the pattern of interdecadal trends shown in Fig 5.17 because these were not constructed independently of the known changes in Sahel rainfall.

5.4.3 Prediction by statistical methods

A further extension of this work has been to demonstrate that relationships very similar to those described above hold between Sahel rainfall and SSTA observed several months in advance, and that there is therfore potential for statistical prediction of the Sahel rainfall. Two methods of prediction are described by Parker et al (1988). The first produces a forecast by creating global fields of regression slopes of SSTA on subsequent Sahel rainfall: an index of the similarity between each year's SSTA field and the regression slope field is then regressed linearly against Sahel rainfall to provide a prediction equation. The second method uses multivariate linear discriminant prediction, a technique also used to make experimental monthly long-range forecasts for the United Kingdom (Folland and Woodcock (1986)). The predictors are selected from the coefficients of the eigenvectors of global SSTA measured several months in advance of the Sahel rainfall season, and, as expected, the coefficients of the third and sixth eigenvectors have been found to dominate the predictors. If SSTA as early as February and March are used, the second

eigenvector (El Nino) also has a beneficial impact on predictive skill, but if later SSTA are used this effect disappears, in accord with the low simultaneous correlations with the second eigenvector reported above. The reason for this decline in influence is likely to be that heat from the mature phase of El Nino has been transmitted into the SSTA fields in the Atlantic and Indian Oceans (Pan and Oort (1983); Wolter (1987)), thus incorporating the aftermath of El Nino into the coefficients of the third and sixth eigenvectors. The quantities predicted by the multivariate linear discriminant method are the probabilities that the Sahel rainfall will be in each of five climatologically equi-probable ranges or "quints". Despite the change in the statistical characteristics of the Sahel rainfall series, both methods showed significant though not consistent skill when used to hindcast years outside the "training periods" used to develop the relationships: see Table 5.1 which is an abridged version of the results of Parker et al (1988). Forecasts issued for 1986 and 1987 correctly indicated very dry years (Fig 5.16), and a prediction of very dry conditions (88% probability of the driest quint) has been issued for 1988.

5.4.4 Advances in the numerical modelling studies

Confidence in the validity of the statistical studies described above has been increased by the results of a series of experiments with an atmospheric general circulation model with an annual cycle (Owen et al (1988)). These experiments used observed fields of SSTA for the wet Sahel years 1950 and 1958 and the dry Sahel years 1983 and 1984, and covered approximately the period April to October inclusive. The first two months were intended to allow the model to adjust to the imposed SSTA from the identical starting conditions, which were those of 26 March 1984. The impact of the SSTA in the model was to give regionally-averaged Sahel rainfall in general accord with observation (Fig 5.22) whether interactive (I) or climatological (C) soil moisture was used (cf Lecture 4). Fig 5.23A is a map of the difference between the simulated rainfall for 1984 and that for 1950, with interactive soil moisture in each case: Fig 5.23B presents the observed differences, which are very similar except that the Guinea coastal region shows a relatively wetter 1984 than was simulated. The rainfall changes in the model were accompanied by a weakened low-level

monsoon flow into the western Sahel (Fig 5.24A) and by weakened upper-tropospheric easterlies over Africa, the Atlantic and the Indian Ocean (Fig 5.24B). The African Easterly Jet centred near 10-15N at 700 mb was strengthened in the model, possibly because of increased heating in the relatively rainless Sahel to the north. The changes in the model when 1983 and 1958 were compared were only slightly weaker, and the results are in accord with the observational study of Newell and Kidson (1984) in which the atmospheric circulation over the Sahel and surrounding areas in dry and wet Sahel years was compared.

A further set of experiments carried out by Owen et al (1988) involved hindcasting Sahel rainfall for the same years by using observed SSTA only up to mid July, then keeping SSTA fixed to simulate a forecasting operation where future SSTA is unspecified. The results were little different from the experiments which used observed SSTA throughout the integrations. Subsequently, an integration using SSTA for April 1988 has produced Sahel rainfall as low as that simulated for 1983 (Fig 5.22).

Finally, experiments were conducted with the SSTA limited to prescribed parts of the globe. When 1984 data were used, extratropical SSTA alone gave results wetter than model climatology, ie their effect was opposite to that observed. However, for 1950 the extratropical SSTA were found to have a more favourable influence than tropical Atlantic SSTA on the skill of the model in simulating Sahel rainfall. This somewhat surprising result is still being assessed.

5.4.5 Atmospheric forcing of the ocean

A noteworthy feature of Fig 5.24A is that, in the model, the wind changes at low levels over the western equatorial Atlantic, when SSTA appropriate to Sahel drought are imposed, are such as to tend to weaken the northward wind-driven surface currents in the ocean off northeastern Brazil. This result has been characteristic of many of the numerical model simulations of Sahel drought conditions (eg Folland et al (1986)), and is in accord with observed differences between the 1950's and the 1970's (Fig 5.25; also Newell and Hsiung (1987)). The significance of these findings is

that most of the oceanic heat flux from the Southern to the Northern Hemisphere takes place in the Atlantic (Charnock (1987); Hsiung (1985)). Thus it is feasible that the wind changes reduce this heat flux and therefore maintain the interhemispheric SSTA contrast (Fig 5.17) which drives them. Alternatively, or additionally, there could have been a weakening of the Indian Ocean heat source which supplies the South Atlantic; or the oceanic circulation of the Atlantic could have been weakened by atmospheric circulation changes over the extratropical North Atlantic (Newell and Hsiung (1987)). Confirmation of these hypotheses will require experiments with models of the ocean, suitably forced by observed atmospheric conditions or, ultimately, interacting with atmospheric general circulation models.

TABLE 5.1 SKILL OF TECHNIQUES FOR PREDICTING SAHEL RAINFALL FROM APRIL AND MAY SST ANOMALIES

Training period	Hindcast period	Persistence of Sahel rainfall in period (autocorrelation with one year's lag)	Regression technique: correlation between forecast and observed values	Discriminant technique: correlation between forecast category and observed category*
1901-45	1946-86	0.69	0.57	0.71
1946-86	1901-45	0.11	0.30	0.34

* Categories are measured on a scale of 1 (very dry) to 5 (very wet)

REFERENCES TO LECTURE 5

BOTTOMLEY, M, FOLLAND, C K, HSIUNG, J, NEWELL, R E and PARKER, D E (1988). Global Ocean Surface Temperature Atlas. Meteorological Office and Massachusetts Institute of Technology. In Press.

CHARNOCK, H (1987) Ocean currents and meridional transfers. Quart J Roy Met, Soc, 113, 3-18.

FOLLAND, C K (1983) Regional-scale interannual variability of climate - a north west European perspective. Met Mag, 112, 163-183.

FOLLAND, C K and COLMAN, A (1988) An interim analysis of the leading covariance eigenvectors of worldwide sea surface temperature anomalies for 1901-80. Long-Range Forecasting and Climate Research LRFC 20, Meteorological Office, Bracknell.

FOLLAND, C K, PALMER, T N and PARKER, D E (1986) Sahel rainfall and worldwide sea temperatures, 1901-85. Nature, 320, 602-607.

FOLLAND, C K and WOODCOCK, A (1986) Experimental monthly long-range forecasts for the United Kingdom. Part I. Description of the forecasting system. Met. Mag., 115, 301-318.

GILL, A E (1982) Atmosphere-ocean dynamics. Academic Press. 664 pp

HASTENRATH, S (1984) Interannual variability and annual cycle: Mechanisms of circulation and climate in the tropical Atlantic sector. Mon Weath Rev, 112, 1097-1107.

HASTENRATH, S (1987) On the prediction of India monsoon rainfall anomalies. J. Clim. Appl. Met. 26, 847-857.

HASTENRATH, S, WU, M-C and CHU, P-S (1984) Towards the monitoring and prediction of north-east Brazil droughts. Quart. J. Roy. Met. Soc, 110, 411-425.

HSIUNG, J (1985) Estimates of global oceanic meridional heat transport. J. Phys. Oceanog., 15, 1405-1413.

KERSHAW, R (1988) The effect of a sea surface temperature anomaly on a prediction of the onset of the south-west monsoon over India. Quart. J. Roy. Met. Soc., 114, 325-345

LAMB, H H (1972) Climate Present, Past and Future, Vol 1. Methuen

LIVEZEY, R E and CHEN, W Y (1983) Statistical field significance and its determination by Monte Carlo techniques. Mon. Weath. Rev 111, 46-59.

LOUGH, J M (1986) Tropical Atlantic sea surface temperatures and rainfall variations in Subsaharan Africa. Mon. Weath. Rev, 114, 561-570.

MONIN, A S (1975) The role of the oceans in climatic models. ICSU/WMO, GARP Publ Ser No 16, Geneva, pp 201-205.

NEWELL, R E and HSIUNG J (1987) Factors controlling free air and ocean temperature of the last 30 years and extrapolation to the past. In "Abrupt Climatic change - Evidence and Implications" (Eds. W H Berger and L D Labeyrie), NATO ASI series C: Mathematical and Physical Sciences, Vol 216, pp 67-87. D Reidel.

NEWELL, R E and KIDSON, J W (1984) African mean wind changes between Sahelian wet and dry periods. J. Climatology, 4, 27-33.

NICHOLSON, S E (1985) Sub-Saharan rainfall 1981-84. J. Clim. Appl. Met, 24, 1388-1391.

OWEN, J A, FOLLAND C K and BOTTOMLEY, M (1988) Numerical simulation of seasonal Sahel rainfall in four past years using observed sea surface temperature. Long-Range Forecasting and Climate Research LRFC 15, Meteorological Office, Bracknell.

PALMER, T N (1985) Response of the UK Meteorological Office general circulation model to sea surface temperature anomalies in the Tropical Pacific Ocean. Coupled Ocean-Atmosphere Models, pp 83-106. Ed: J Nihoul, Elsevier.

PALMER, T N (1986) Influence of the Atlantic, Pacific and Indian Oceans on Sahel rainfall. Nature, 322, 251-253.

PALMER, T N (1988) Medium and extended range predictability and stability of the Pacific North American mode. Quart. J. Roy. Met. Soc., 114, 691-713

PALMER, T N and MANSFIELD, D A (1986a) A study of wintertime circulation anomalies during past El Nino events using a high resolution general circulation model. I. Influence of model climatology. Quart. J. Roy. Met. Soc., 112, 613-638.

PALMER, T N and MANSFIELD, D A (1986b) A study of wintertime circulation anomalies during past El Nino events using a high resolution general circulation model. II. Variability of the seasonal mean response. Quart. J. Roy. Met. Soc., 112, 639-660.

PALMER, T N and SUN-Z (1985) A modelling and observational study of the relationship between sea surface temperature in the North West Atlantic and the atmospheric general circulation. Quart. J. Roy. Met. Soc., 111, 947-975.

PAN, Y H and OORT, A H (1983) Global climate variations connected with sea surface temperature anomalies in the eastern equatorial Pacific Ocean for the 1958-73 period. Mon. Weath. Rev., 111, 1244-1258.

PARKER, D E (1982) Large-scale interannual variability of climate. Met. Mag., 111, 193-208.

PARKER, D E and FOLLAND, C K (1988) The nature of climatic variability. Met. Mag., 117, 201-210.

PARKER, D E, FOLLAND, C K and WARD, M N (1988) Sea surface temperature anomaly patterns and the prediction of seasonal rainfall in the Sahel region of Africa. In "Recent Climatic Change - A Regional Approach", Ed. S. Gregory, Belhaven Press, pp 166-178.

RATCLIFFE, R A S and MURRAY, R (1970) New lag associations between North Atlantic sea temperature and European pressure applied to long-range weather forecasting. Quart. J. Roy. Met. Soc., 96, 226-246.

ROWNTREE, P R (1976) Response to the atmosphere to a tropical Atlantic ocean temperature anomaly. Quart. J. Roy. Met. Soc., 102, 607-626.

ROWNTREE, P R (1984) A survey of ocean surface temperature anomaly experiments for the Northern Hemisphere winter. Met O 20 Technical Note II/220.

SAWYER, J S (1965) Notes on the possible physical causes of long-term weather anomalies. WMO Tech Note, No 66, pp 227-48, Geneva.

SIMMONS, A J (1982) The forcing of stationary wave motion by tropical diabatic heating. Quart. J. Roy. Met. Soc., 108, 503-534.

SMAGORINSKY, J (1953) The dynamical influence of large-scale heat sources and sinks on the quasi-stationary mean motions of the atmosphere. Quart. J. Roy. Met. Soc., 79, 342-366.

WARD, M N, BROOKS, S and FOLLAND, C K (1988) Predictability of seasonal rainfall in the Nordeste region of Brazil. In "Recent climatic change - a regional approach", Ed S Gregory, Belhaven Press, pp 237-251.

WOLTER, K (1987) The Southern Oscillation in surface circulation and climate over the tropical Atlantic, eastern Pacific and Indian Ocean as captured by cluster analysis. J. Clim. Appl. Met., 26, 540-558.

WOODRUFF, S D, SLUTZ, R J, JENNE, R L and STEURER, P M (1987) A Comprehensive Ocean-Atmosphere Data Set. Bull. Amer. Met. Soc., 68, 1239-1250.

The world map of annual range of surface temperature.
(After Monin 1975.)

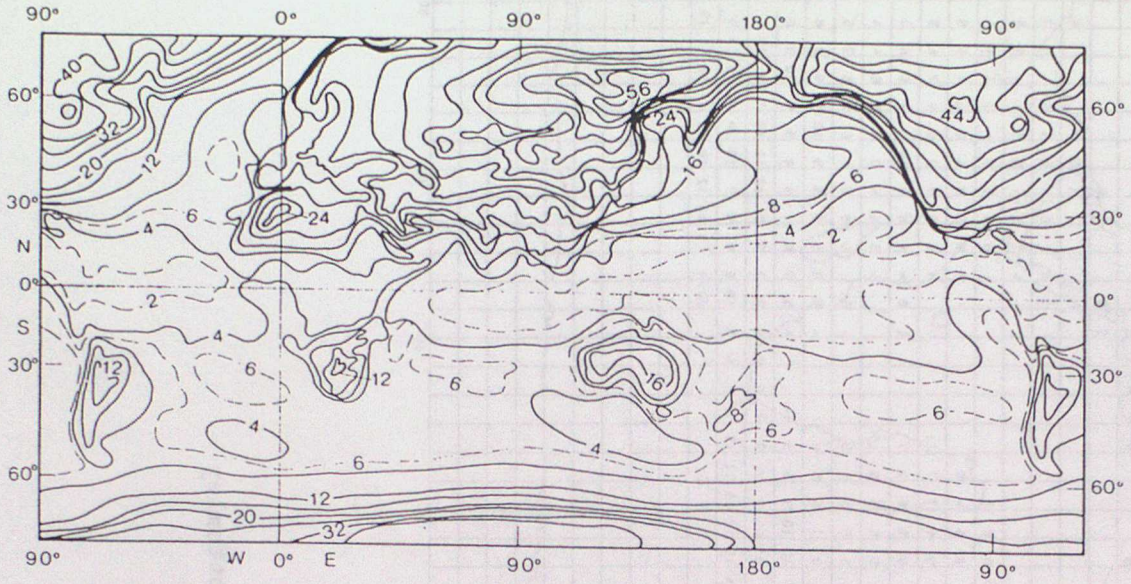

Figure 5.1.

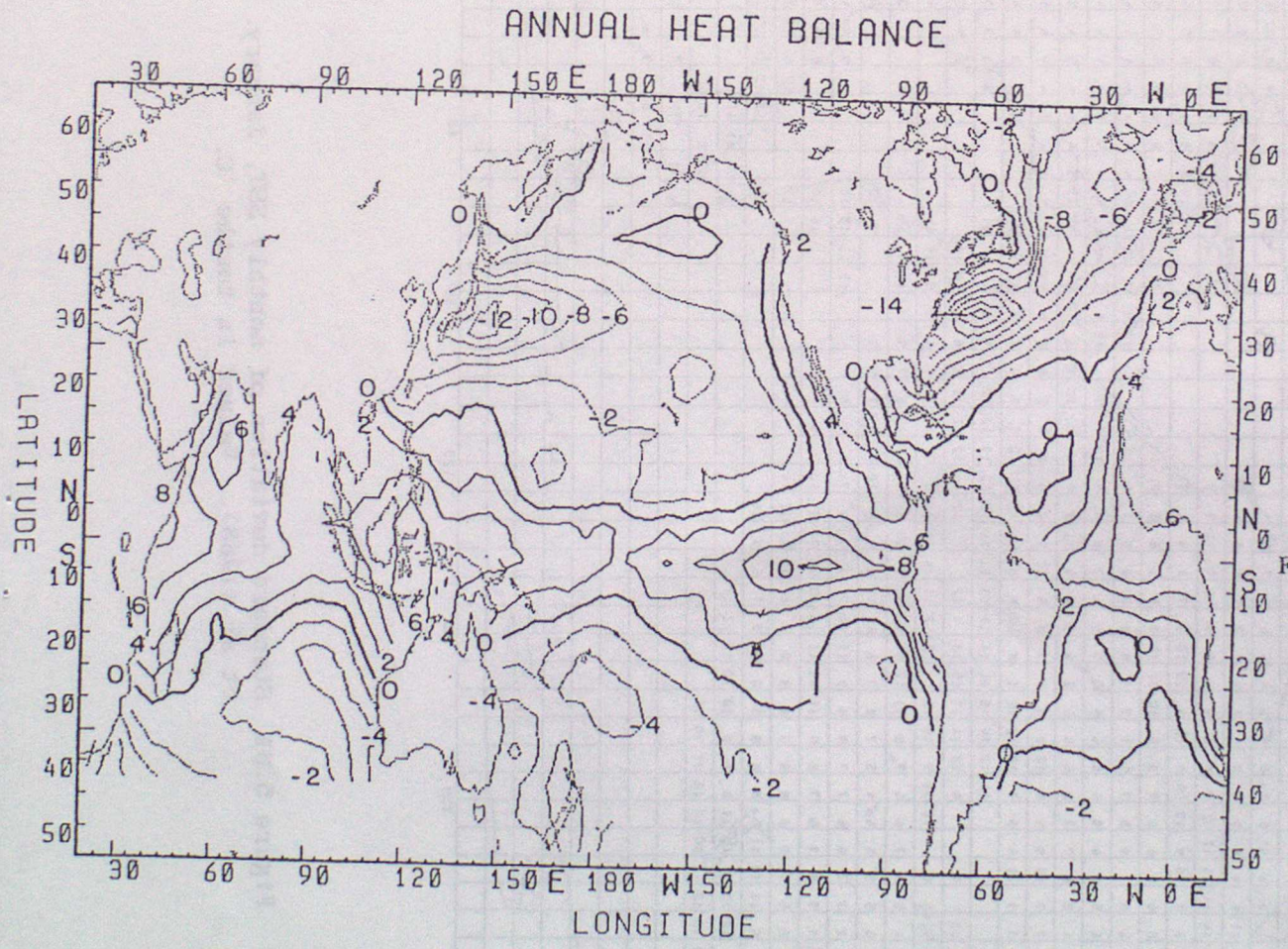

The annual mean net energy balance at the surface. The units are in W m^{-2} when multiplied by 10.

Figure 5.2
From Hsiung (198

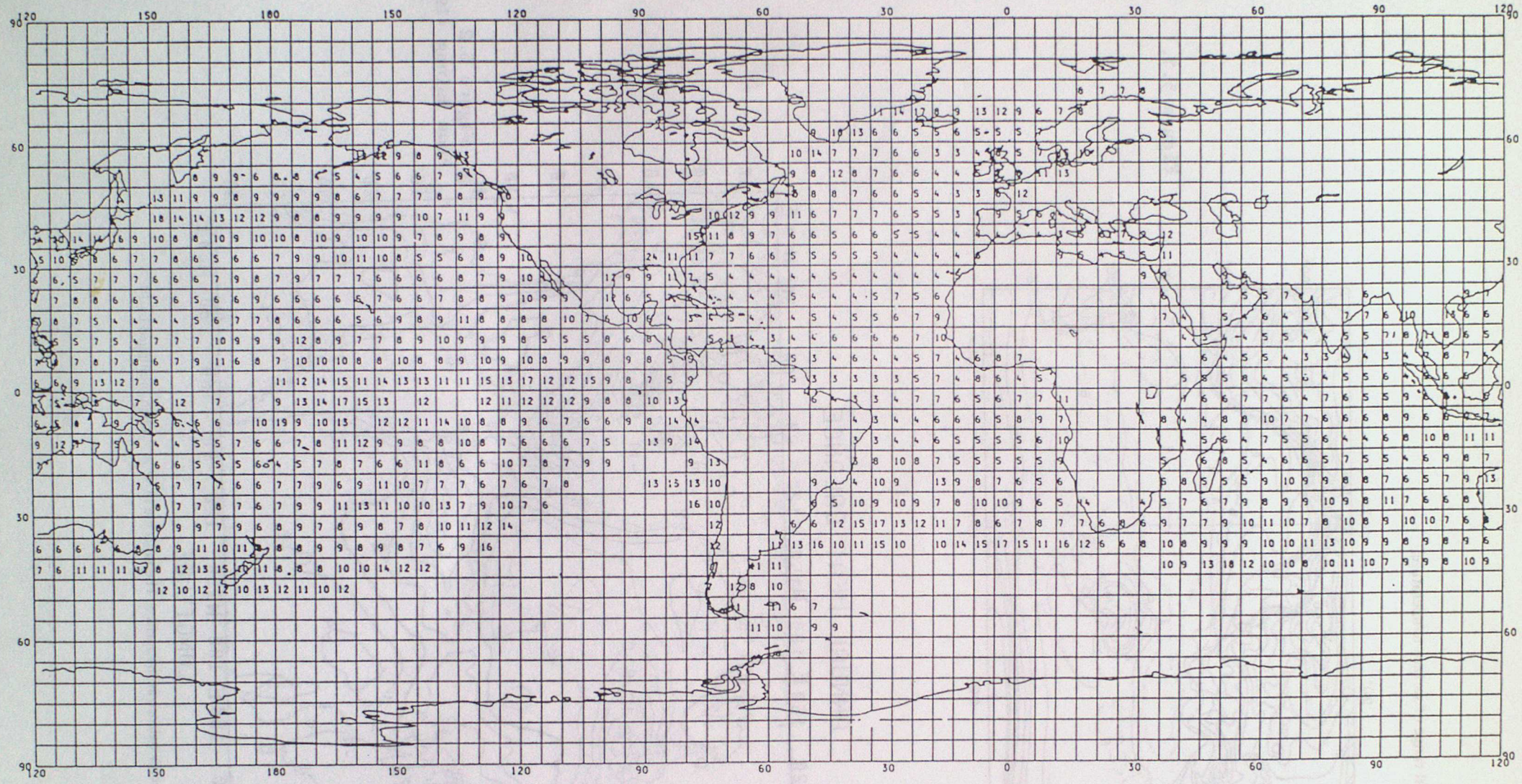

Figure 5.3A Standard deviation of monthly SST, January. After Bottomley et al (1988). Values in tenths °C.

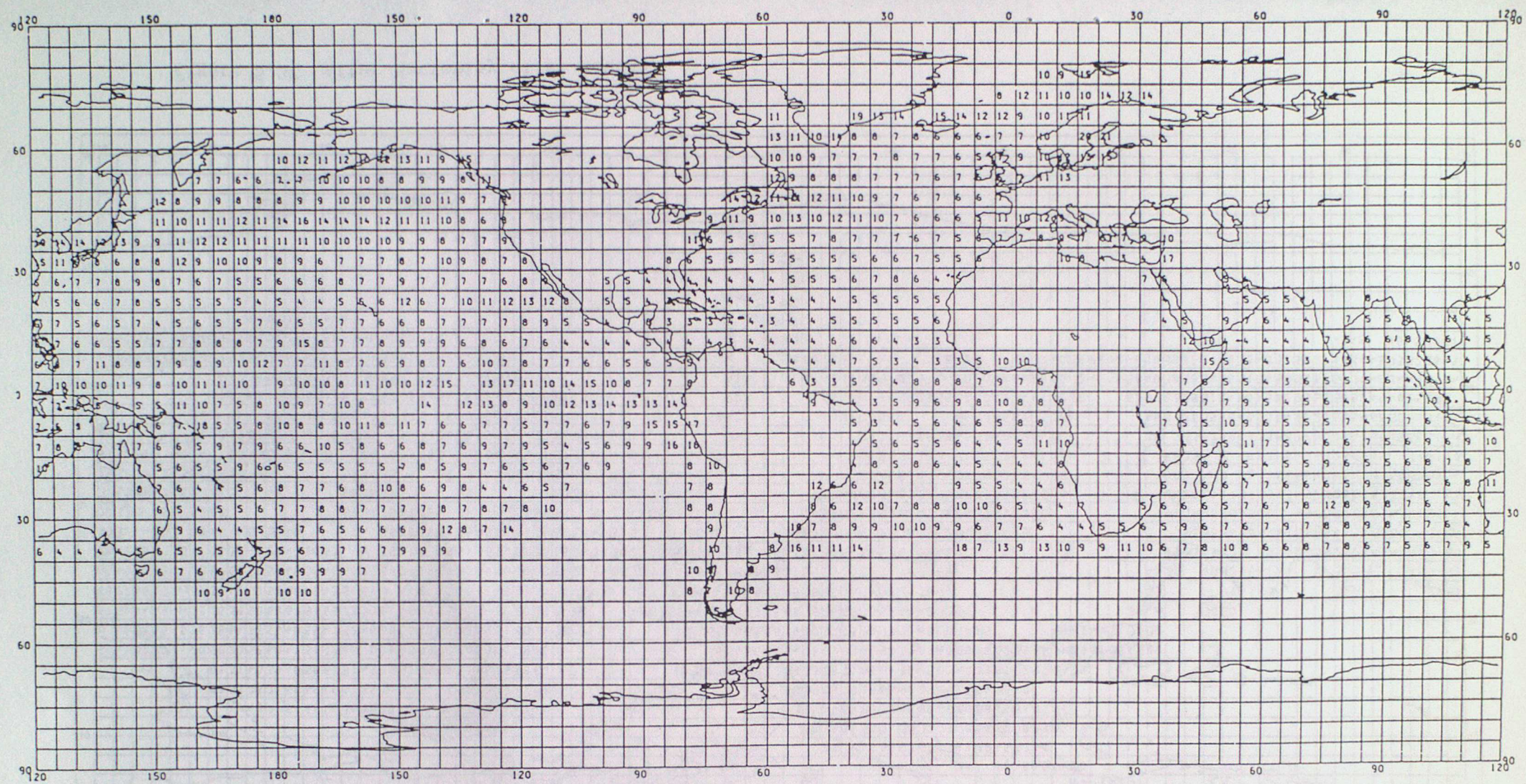

Figure 5.3B Standard deviation of monthly SST, July.
After Bottomley et al (1988). Values in tenths °C.

ONE MONTH LAG CORRELATIONS OF SST ANOMALY FOR FEBRUARY - JANUARY

CORRELATIONS ARE *100

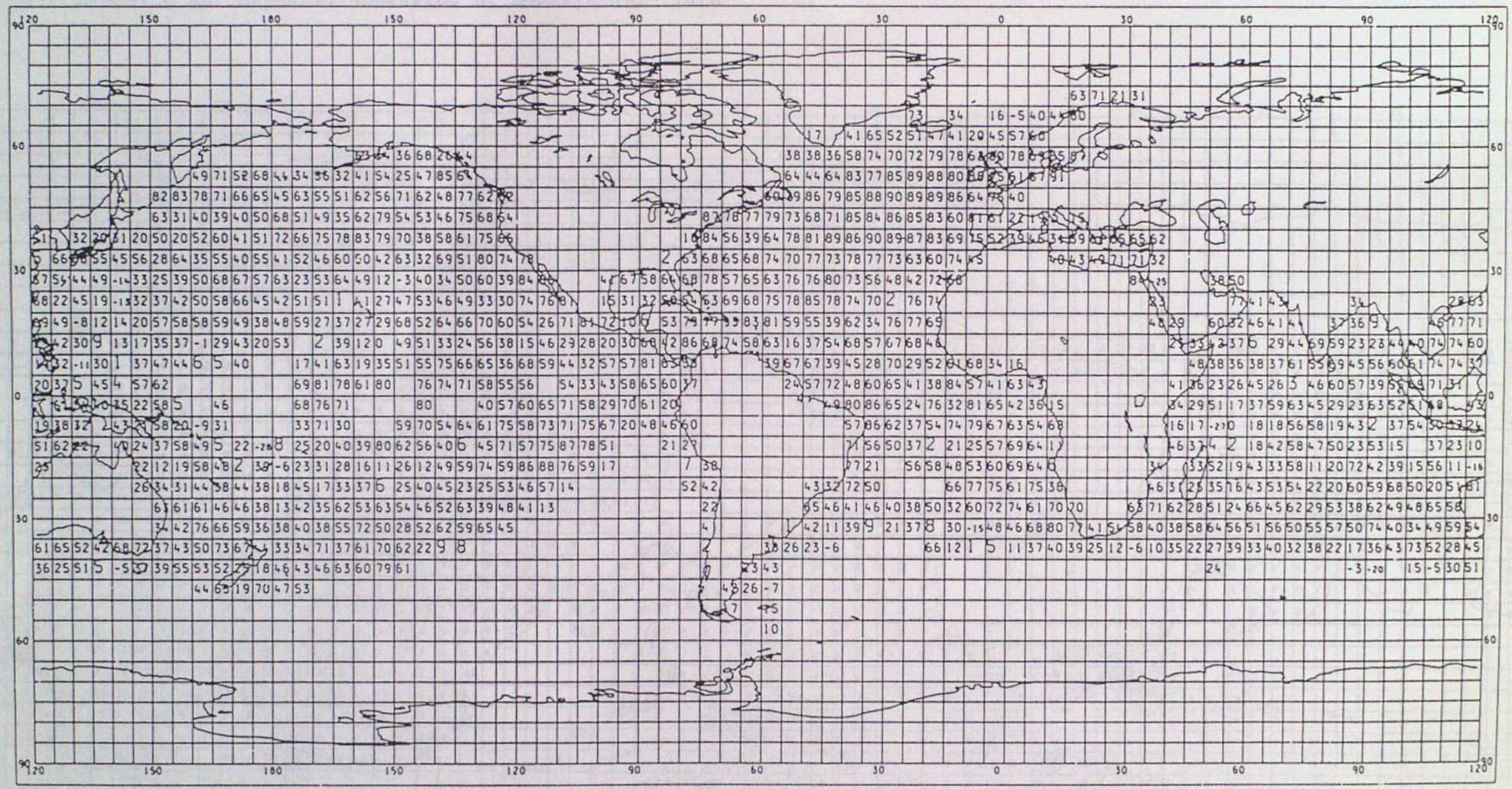

Figure 5.3C After Bottomley et al (1988).

ONE MONTH LAG CORRELATIONS OF SST ANOMALY FOR AUGUST - JULY

CORRELATIONS ARE ×100

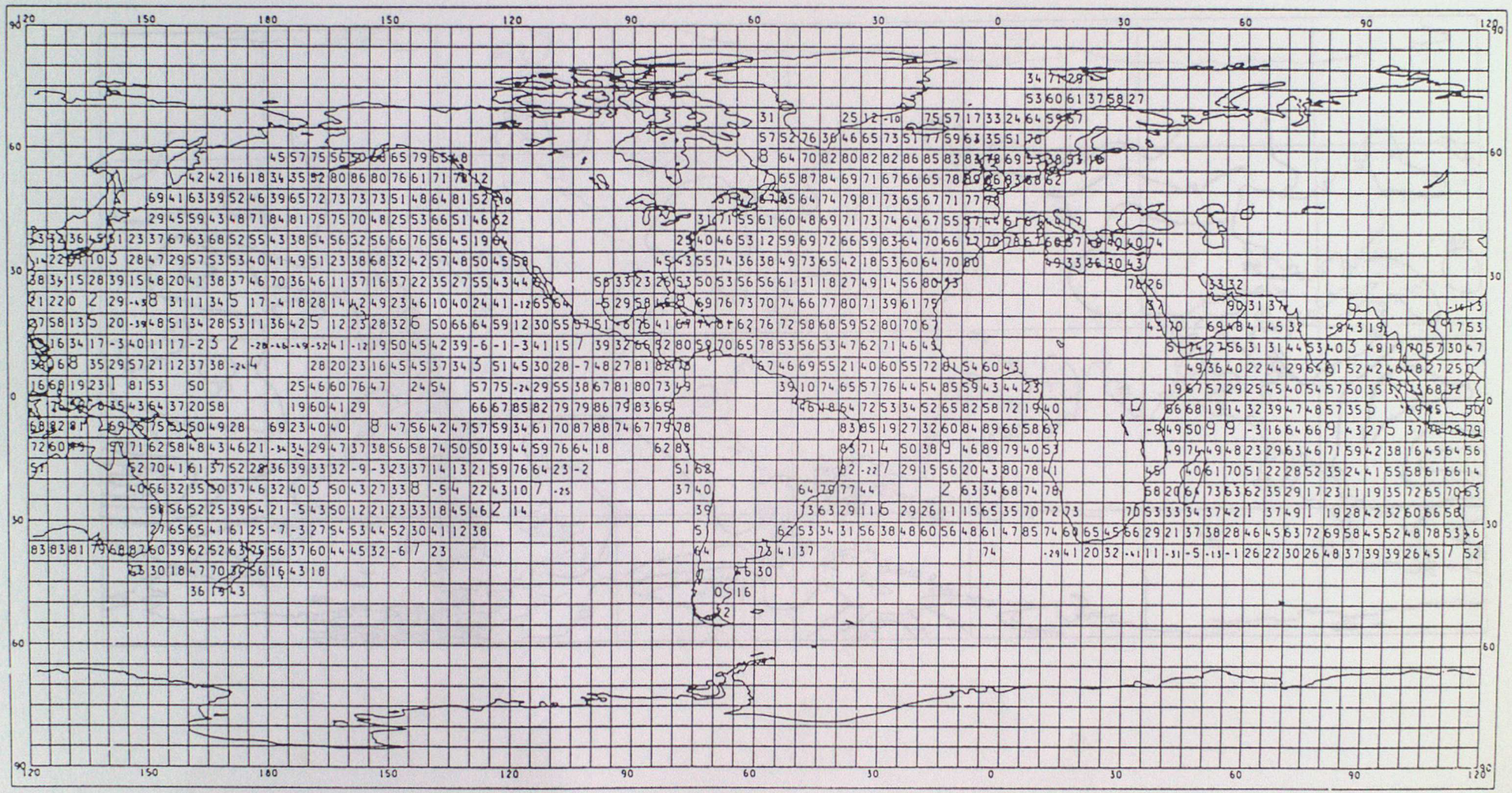

Figure 5.3D After Bottomley et al (1988)

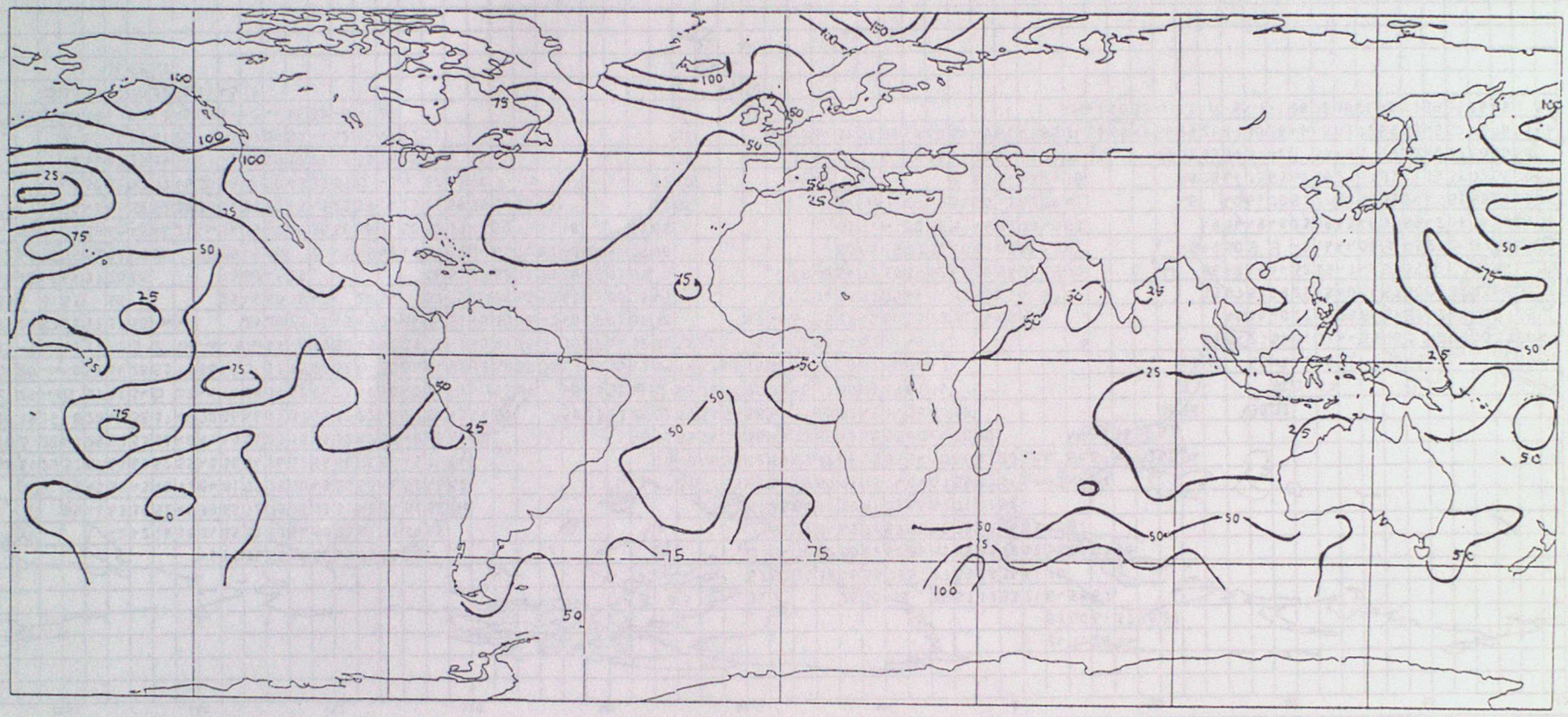

Figure 5.4A. The first all-seasons covariance eigenvector of global SSTA, 1901-80. The pattern is scaled so that the sum of squares of 10^{o} latitude x longitude values equals 10^{6}.

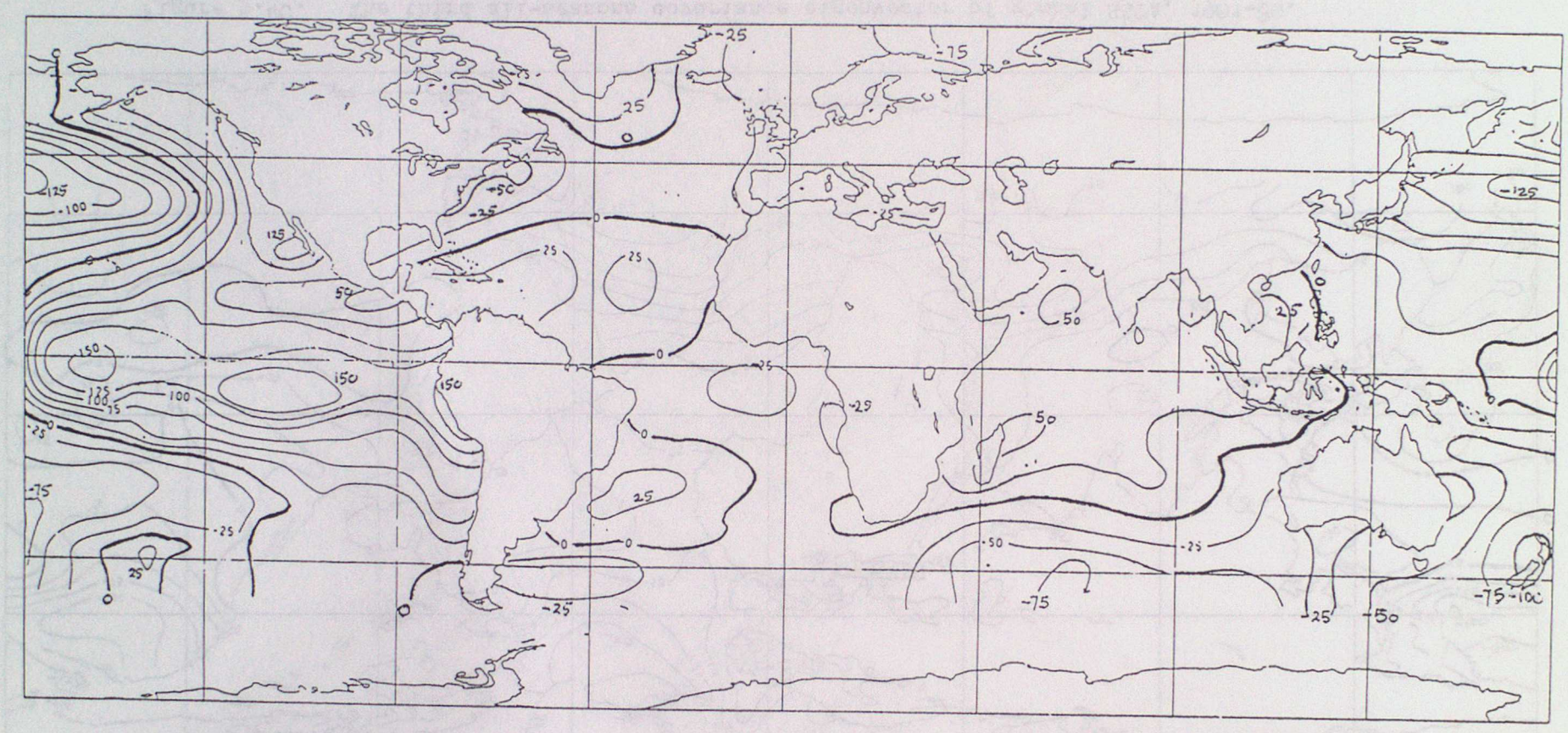

Figure 5.4B. The second all-seasons covariance eigenvector of global SSTA, 1901-80. Scaling as in Fig. 5.4A.

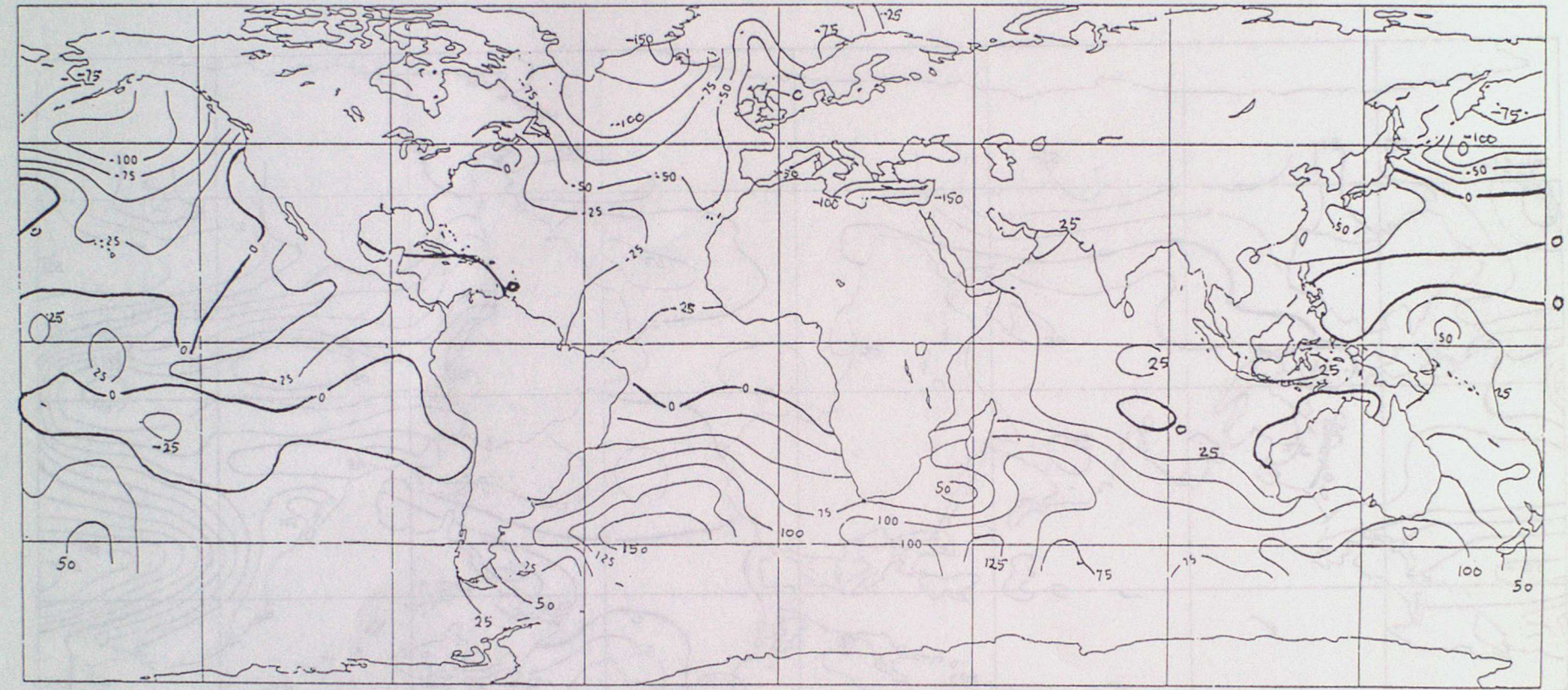

Figure 5.4C. The third all-seasons covariance eigenvector of global SSTA, 1901-80. Scaling as in Fig. 5.4A.

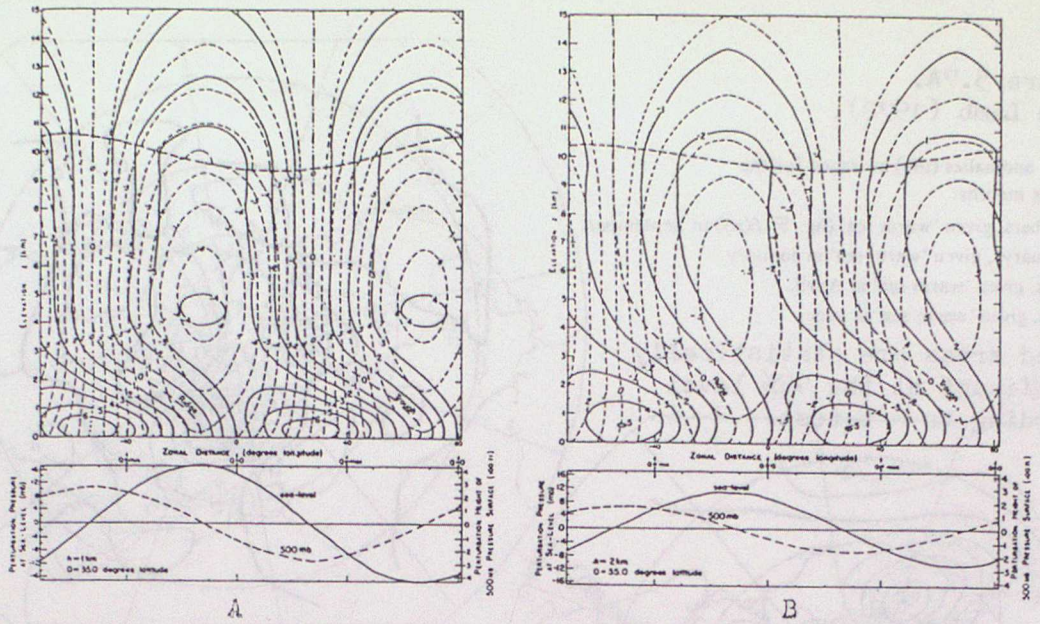

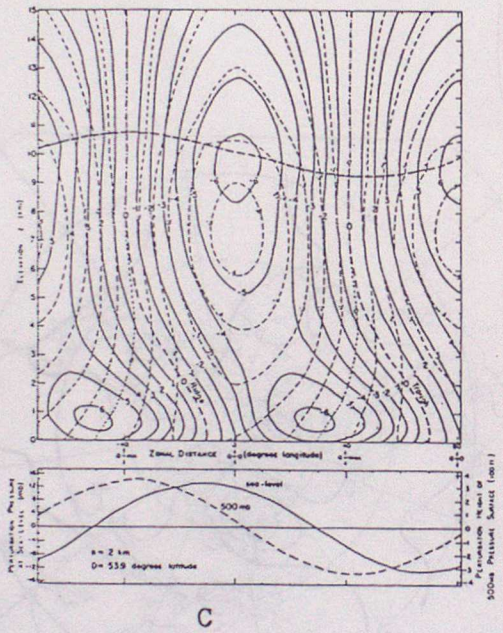

Figure 5.5.

General baroclinic model with surface friction, at latitude of maximum heating and cooling. Stable stratosphere taken into account. Upper part : zonal section of perturbation meridional velocity v (solid lines) in m sec^{-1} and perturbation vertical velocity w (dashed lines) in cm sec^{-1}. Lower part : zonal profile of perturbation pressure at sea level (solid lines) and perturbation height of 500-mb pressure surface (dashed lines).

From Smagorinsky (1953)

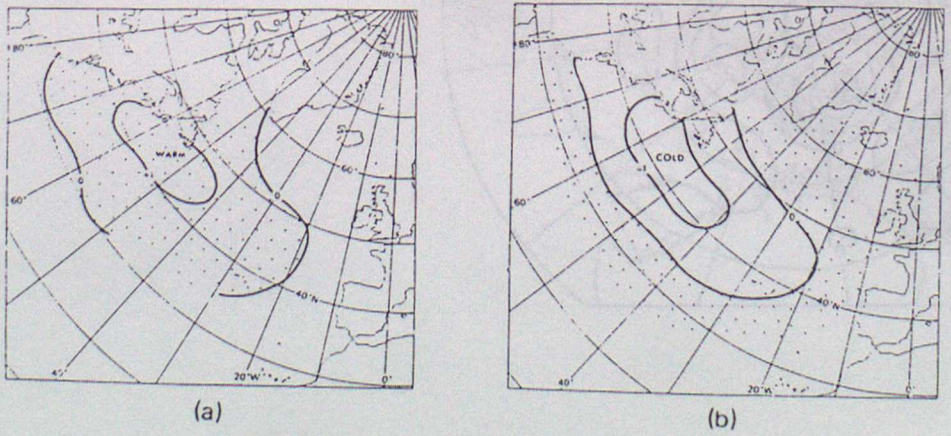

Generalized sea surface temperature anomaly distributions (°C):
(*a*) Type here designated as 'warm sea' cases.
(*b*) Type here designated as 'cold sea' cases.

Figure 5.6. From Lamb (1972).

Figure 5.7A.
From Lamb (1972).

Pressure anomalies (mb) averaged for the following months:

(*a*) Octobers, given 'warm sea' (fig. 5.6(*a*)) in September.

(*b*) Februarys, given 'warm sea' in January.

(*c*) Mays, given 'warm sea' in April.

(*d*) Julys, given 'warm sea' in June.

Shaded areas are statistically significant at the 95% level ~~according to a t-test.~~

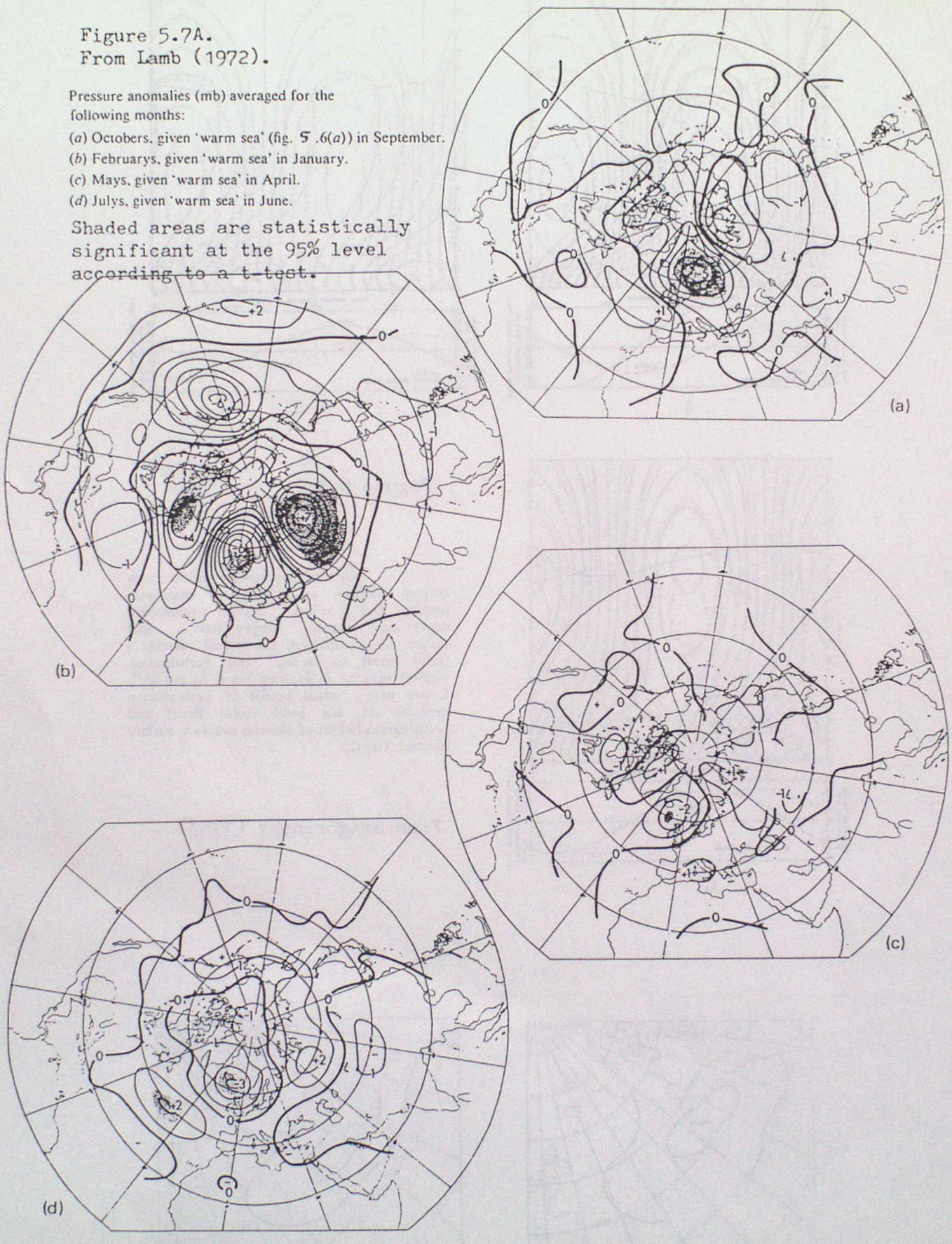

Figure 5.7B.
From Lamb (1972).

Pressure anomalies (mb) averaged for the following months:

(*a*) Octobers, given 'cold sea' (fig. 5.6(*b*)) in September.
(*b*) Februarys, given 'cold sea' in January.
(*c*) Mays, given 'cold sea' in April.
(*d*) Julys, given 'cold sea' in June.

Shading as in Fig 5.7A.

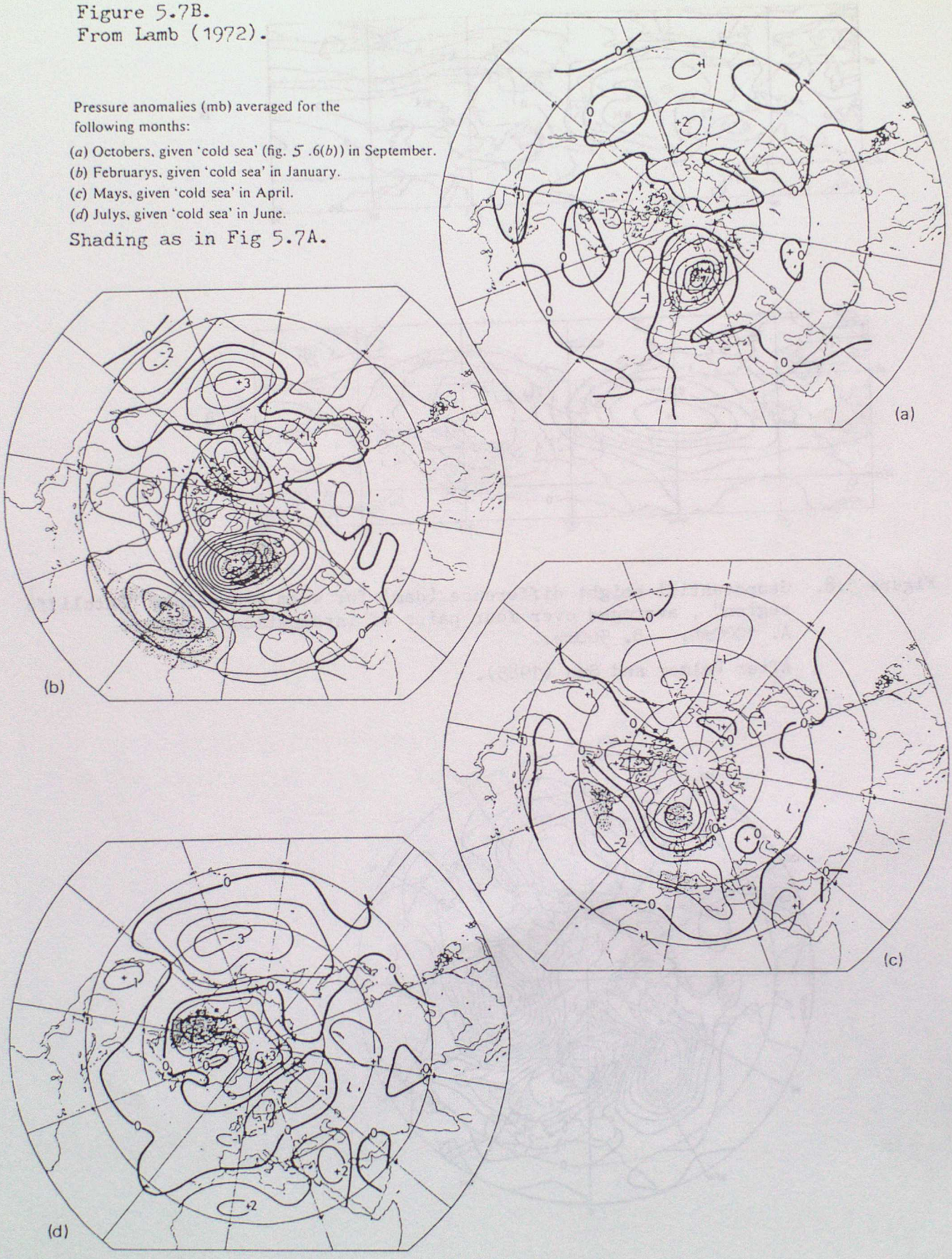

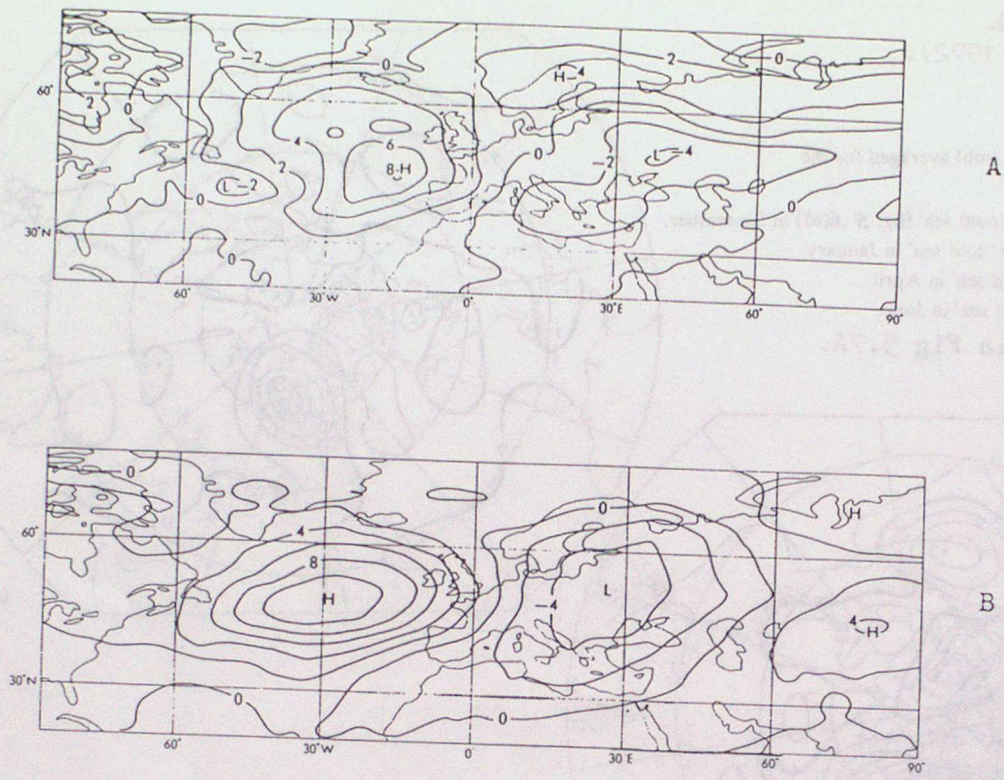

Figure 5.8. Geopotential height difference (dam) for warm minus cold "Ratcliffe region" , averaged over four pairs of integrations. Winter.
A. 1000mb. B. 500mb.

After Palmer and Sun (1985).

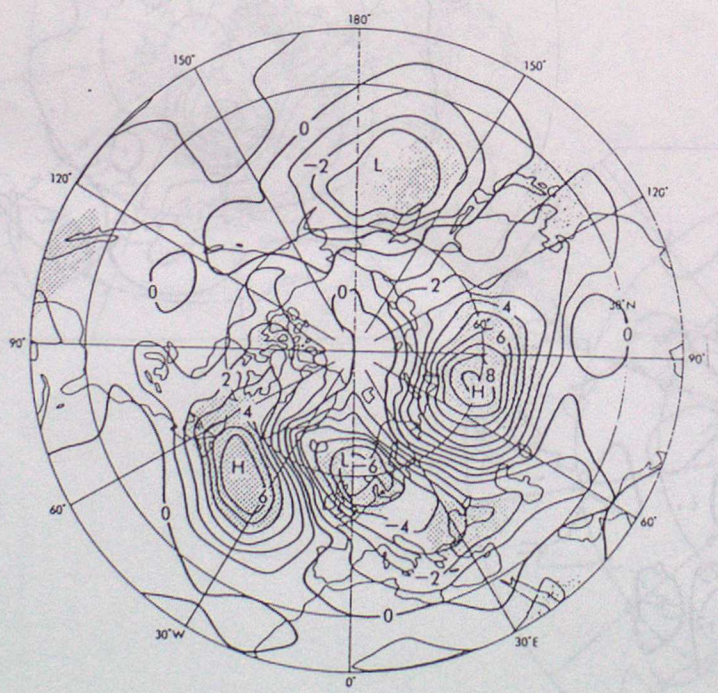

Figure 5.9 Observed synchronous MSL pressure difference (mb) for warm minus cold "Ratcliffe region" averaged over November to February 1951-80. Shading as in Fig. 5.7.
After Palmer and Sun (1985).

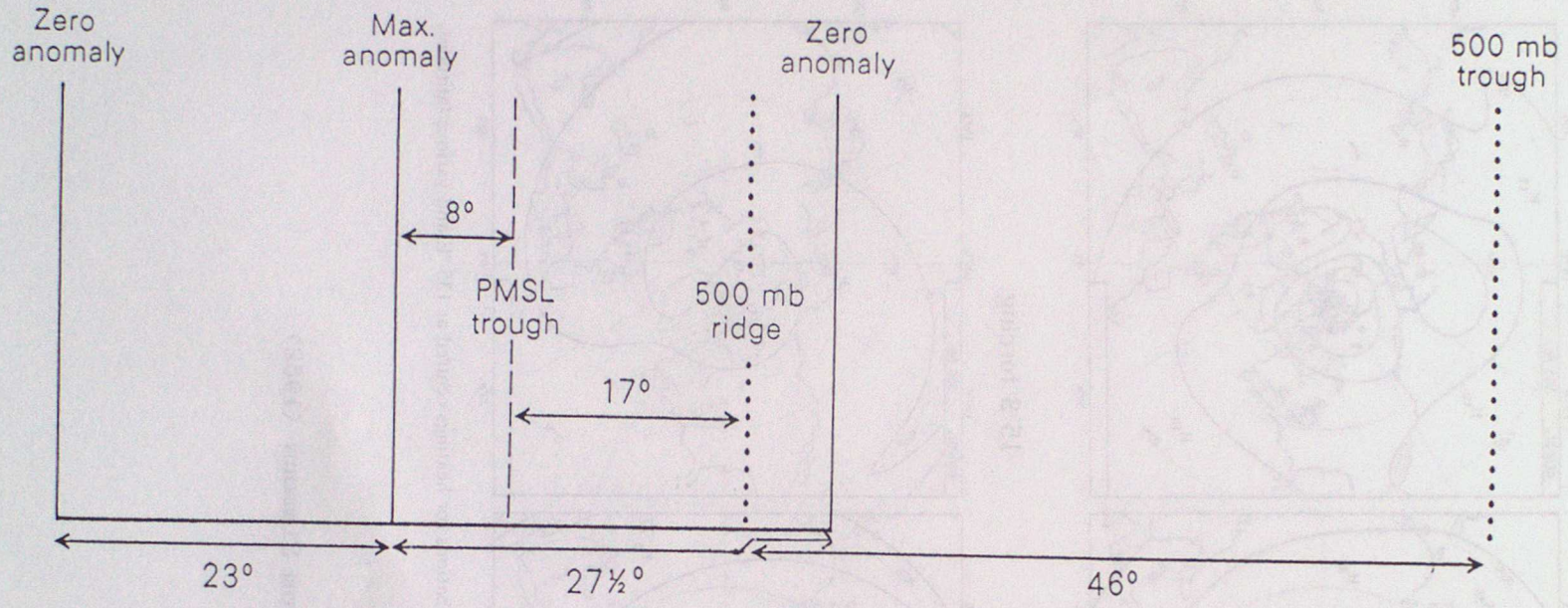

Summarised effects of warm mid-latitude SST anomalies on PMSL and 500 mb height (from Rowntree 1984)

Figure 5.10.

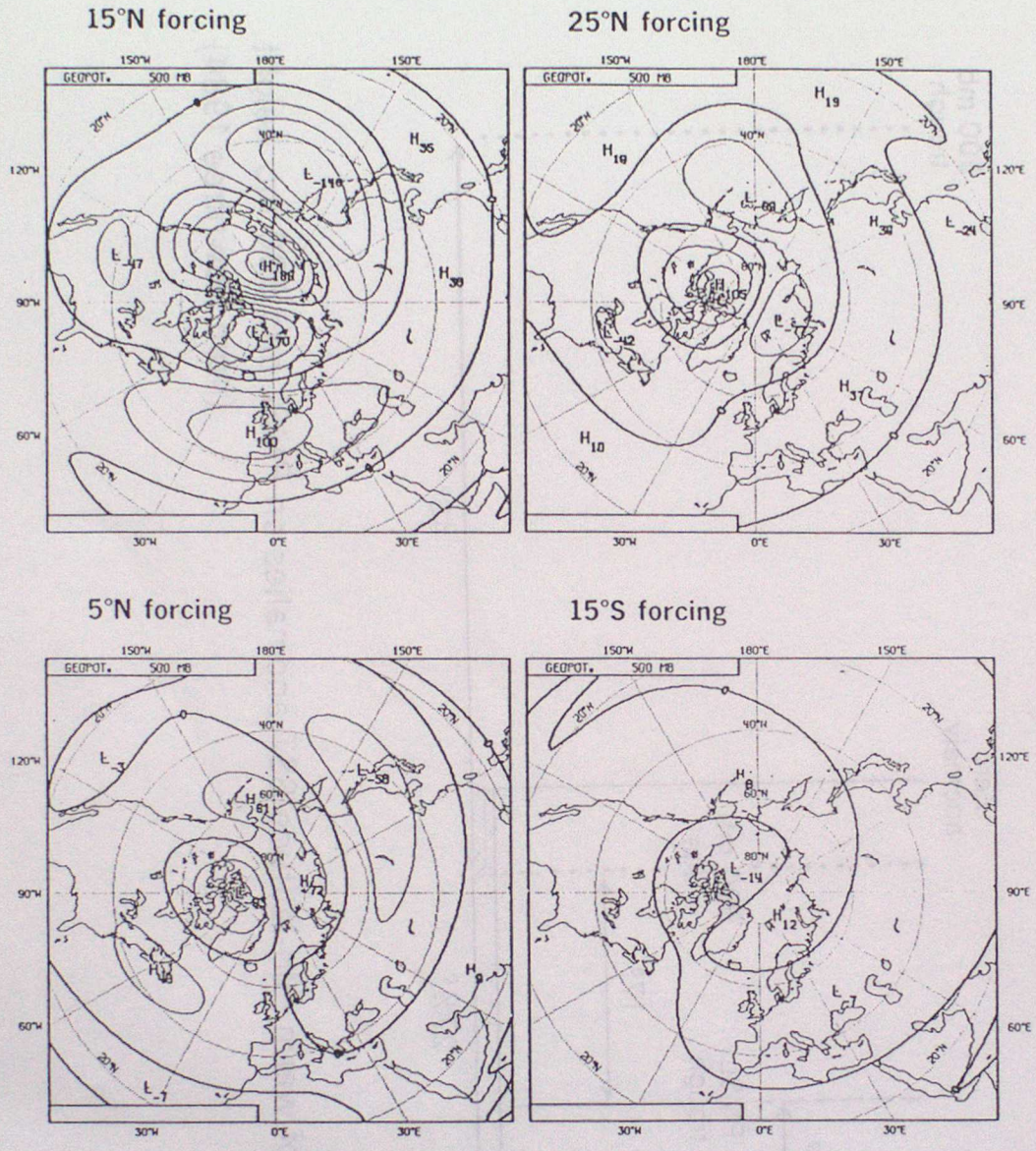

500 mb height perturbations for heatings centred at 135 °E and various latitudes.

January.

Figure 5.11. From Simmons (1982)

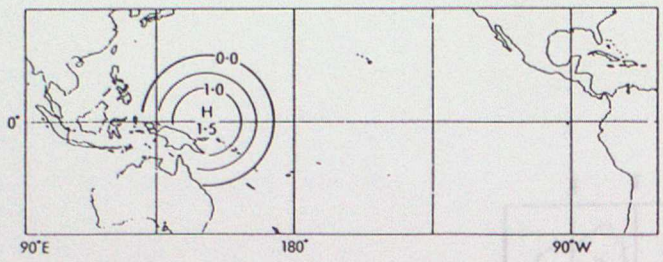

Figure 5.12A. West Pacific SST anomaly (°C) used by Palmer and Mansfield (1986b)

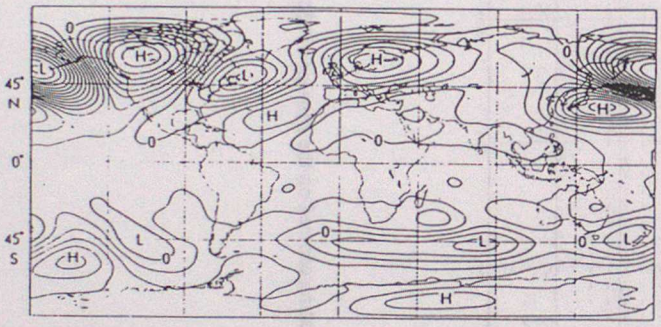

Figure 5.12B. 250mb geopotential height anomaly produced by the model of Palmer and Mansfield (1986b) in response to the SST anomaly shown in Fig. 5.12A
This was a 540-day "perpetual January" experiment.

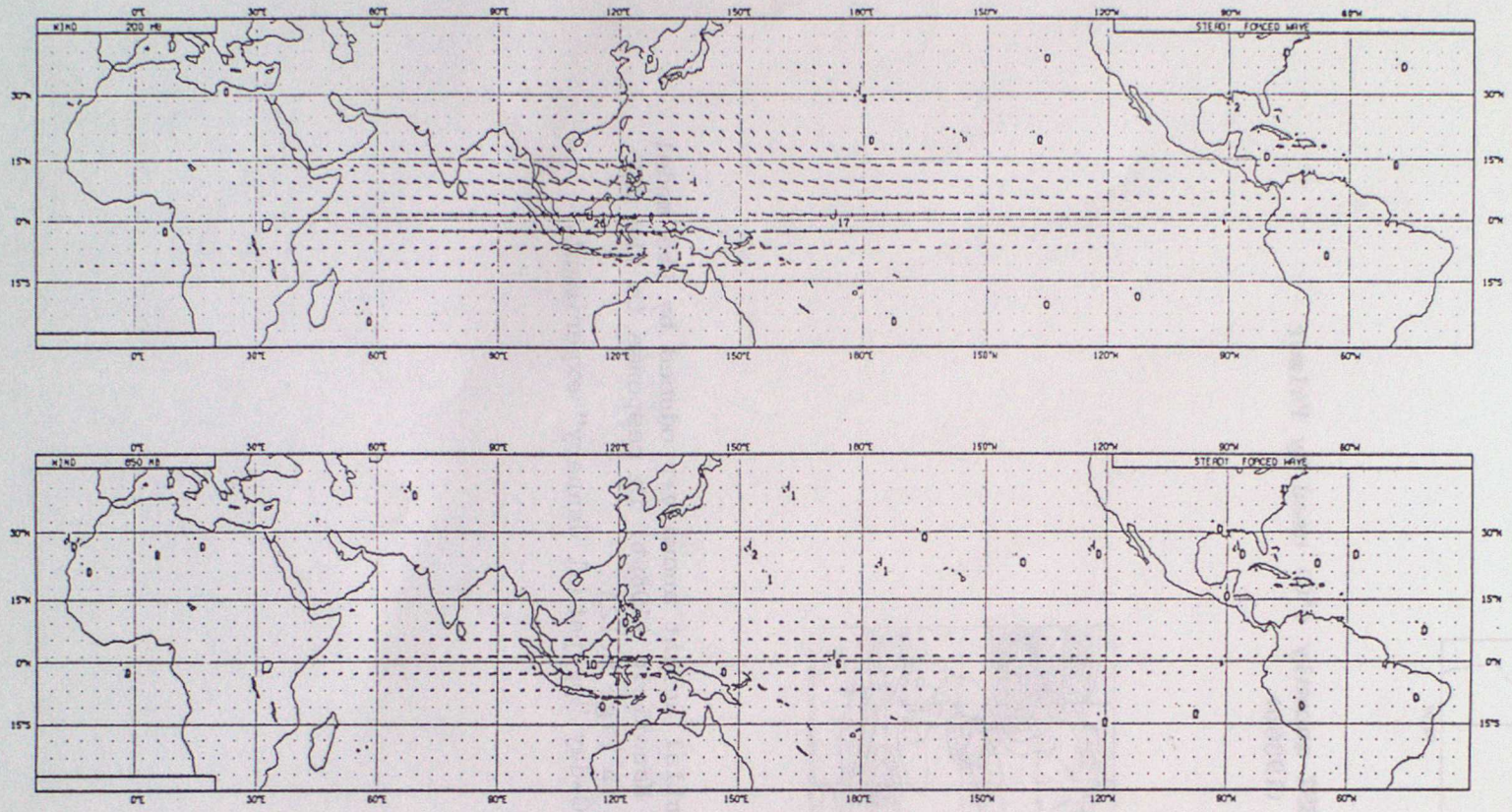

Perturbation winds at 200 mb and 850 mb for a heating centred on the equator at 135 °E. Velocity maxima (in $m\,s^{-1}$) are marked.

Figure 5.13. From Simmons (1982).

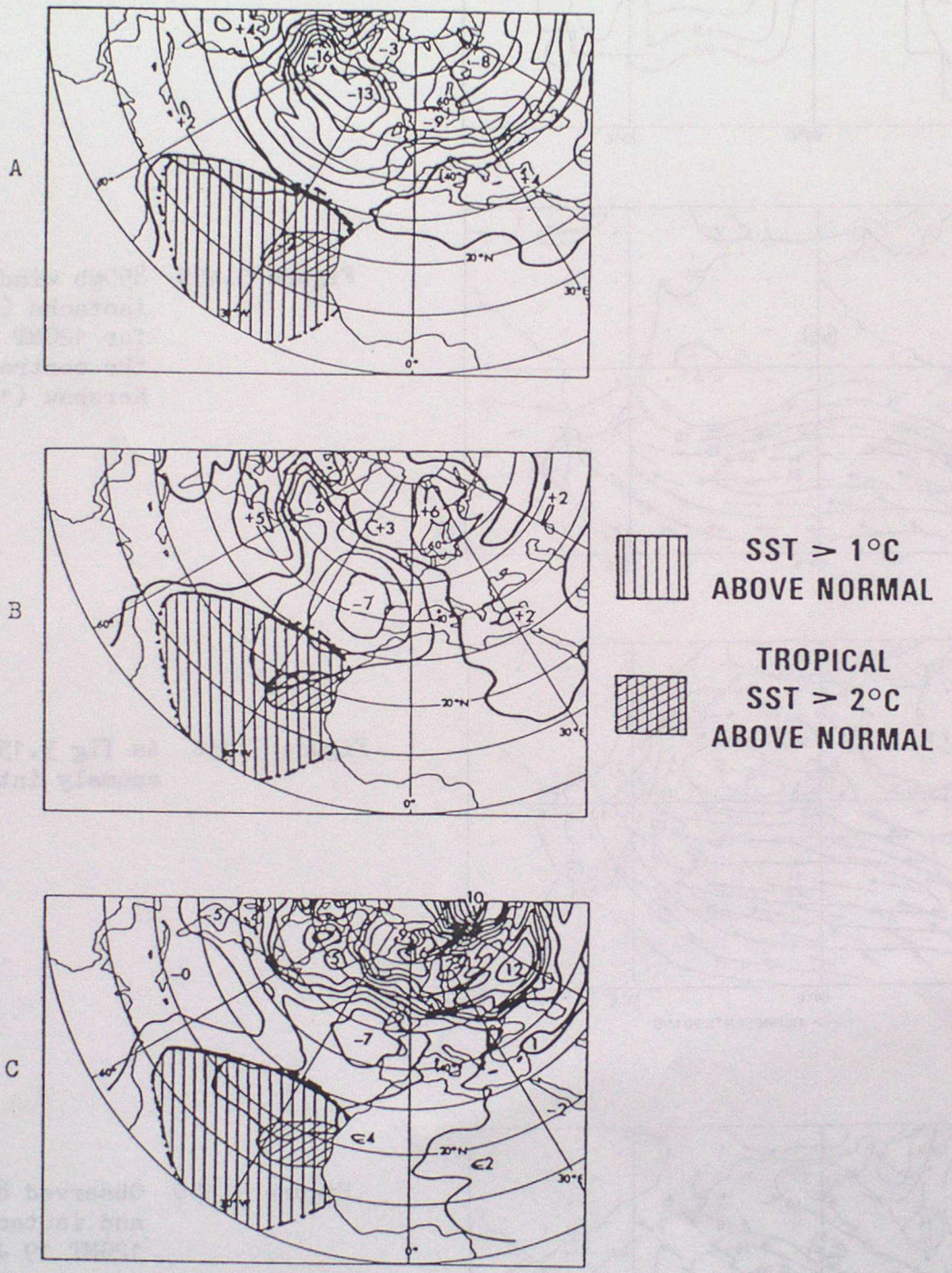

Difference in mean surface pressure (mb) averaged over days 41–80 of model integrations between surface pressure obtained with tropical Atlantic warming and the control experiment without the warming. (A) experiment 1 using isothermal initial data, (B) experiment 2 using initial real data, and (C) experiment 3 also using initial real data. Both (B) and (C) use initial data for 29 December 1965. SST averages taken from US Naval Oceanographic Office data.

Figure 5.14. Taken from Rowntree (1976) by Folland (1983).

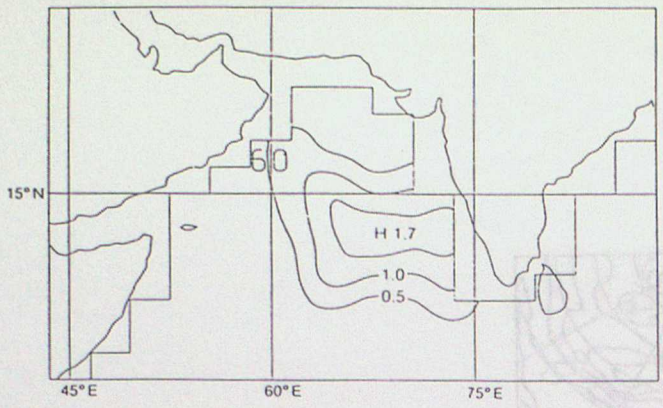

Figure 5.15A SST anomaly used by Kershaw (1988)

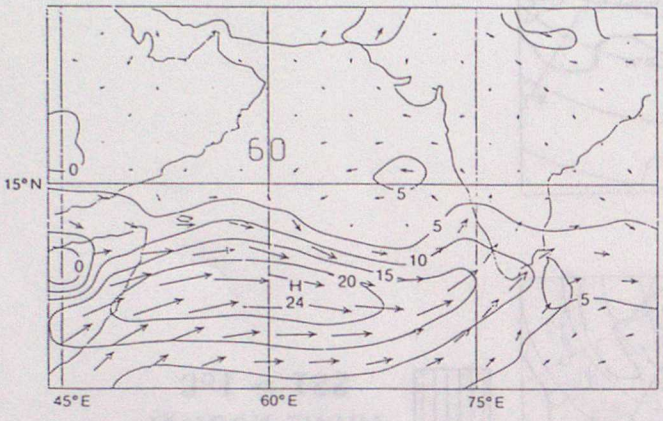

Figure 5.15B 850mb wind vectors and isotachs (m/sec) predicted for 12GMT 19 June 1979 in the control integration of Kershaw (1988)

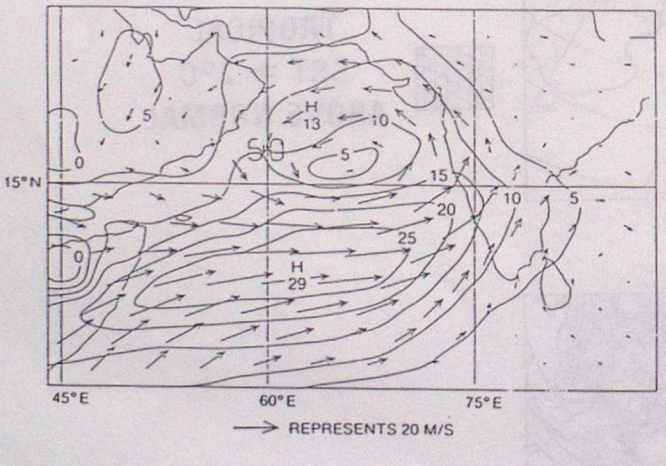

Figure 5.15C As fig 5.15B but for the anomaly integration

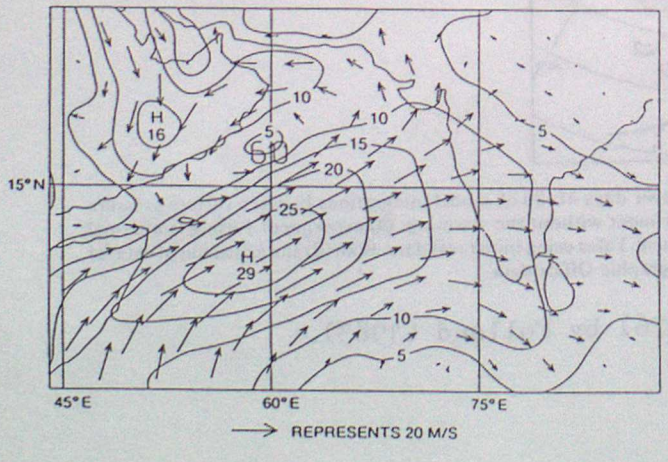

Figure 5.15D Observed 850mb wind vectors and isotachs (m/sec) for 12GMT 19 June 1979

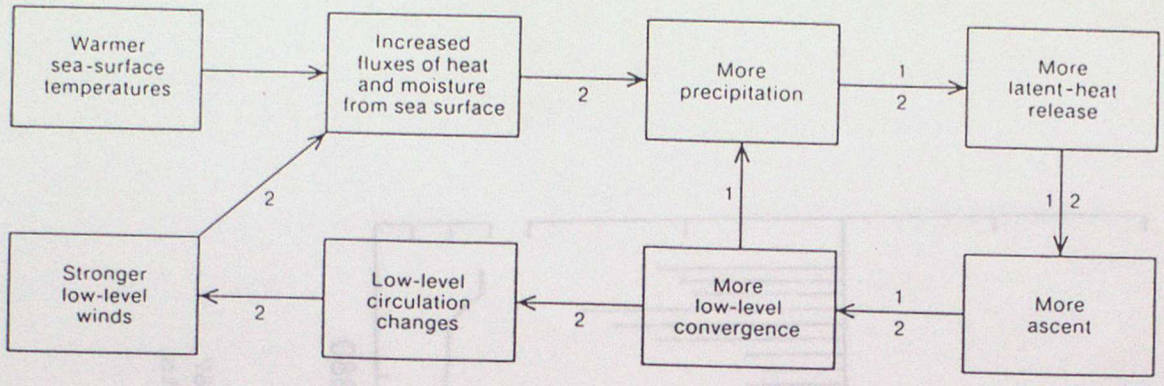

Figure 5.15 E Two feedback loops relating an Arabian sea SST anomaly to atmospheric changes associated with the Indian Monsoon onset. After Kershaw (1988)

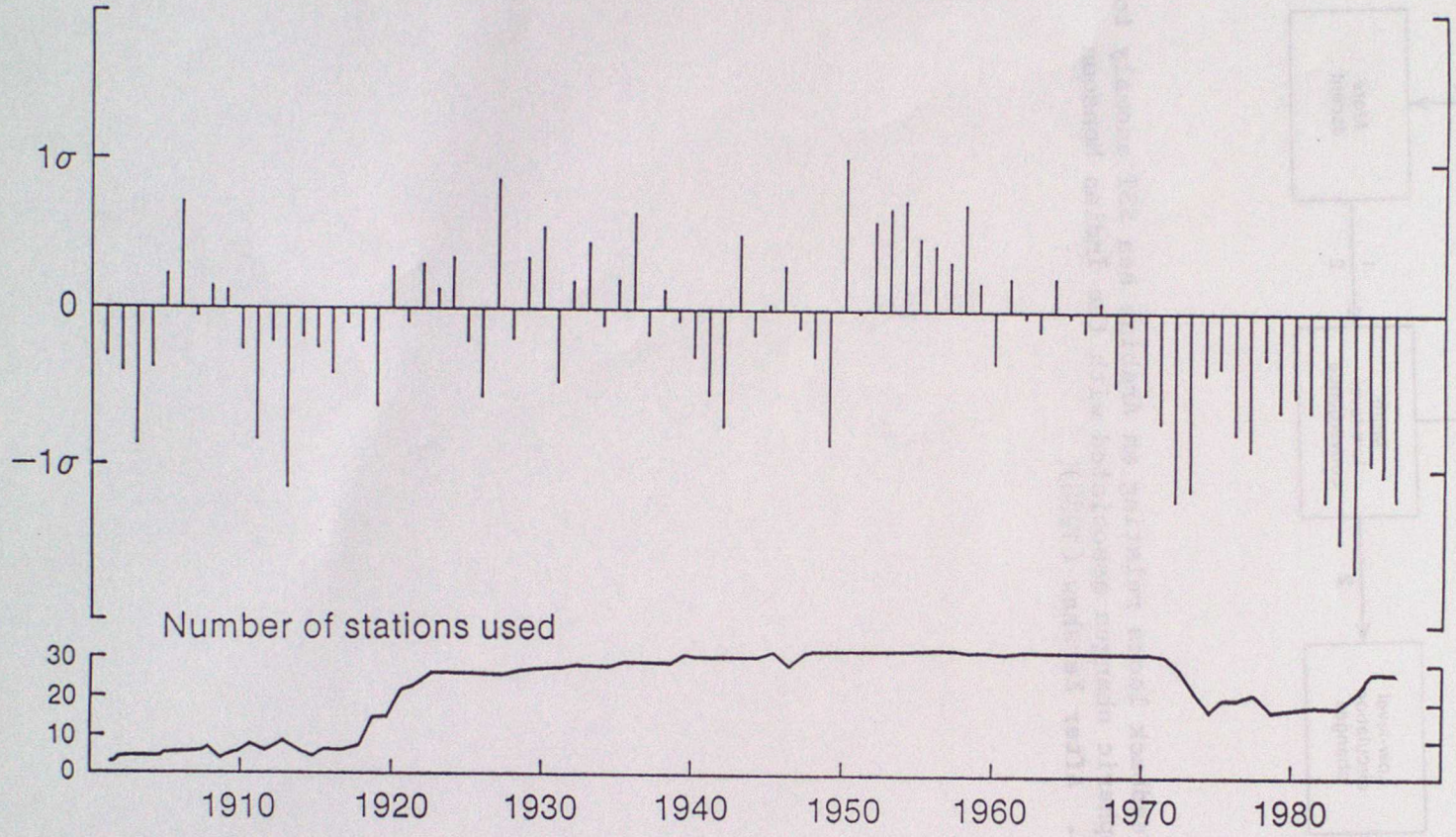

Figure 5.16. Standardised annual rainfall anomalies for the Sahel, 1901-87. Values to 1984 after Nicholson (1985): 1985-87 estimated from CLIMAT reports.

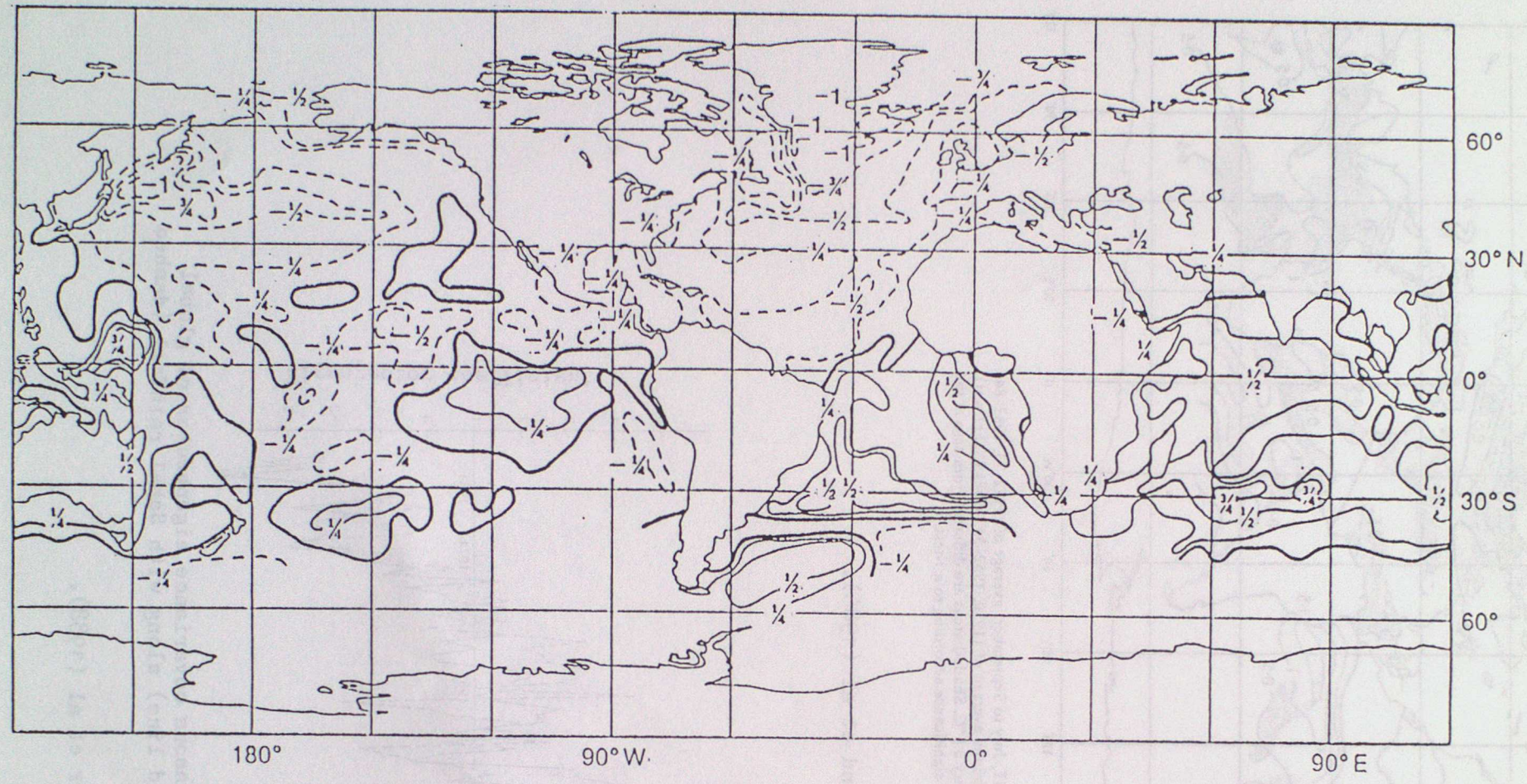

Mean sea surface temperature difference (°C) for 1971–1987 relative to 1951–60.

Figure 5.17. From Parker and Folland (1988).

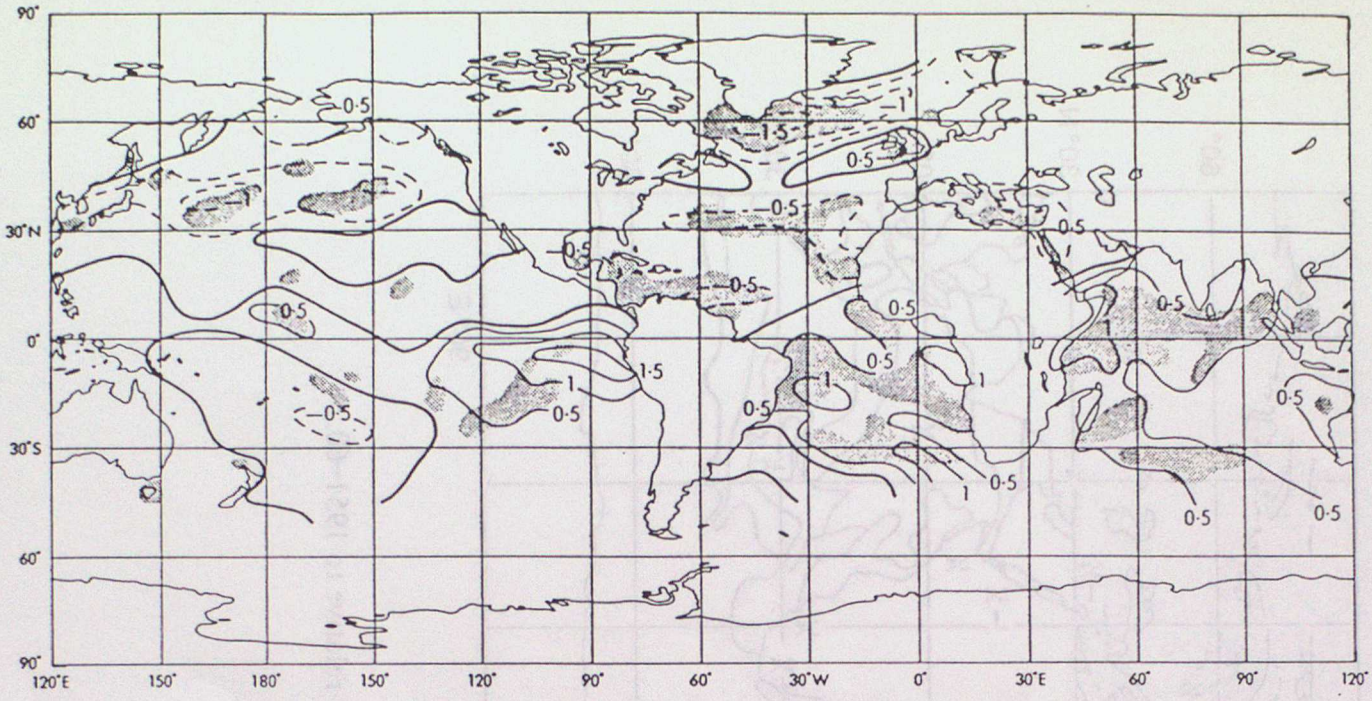

a, SST, July to September: average of (1972–73, 1982–84) (Sahel dry) minus average of (1950, 1952–54, 1958) (Sahel wet). Contours every 0.5 °C. Shaded areas are different from zero at the 90% level of significance according to a *t*-test.

Figure 5.18. From Folland et al (1986).

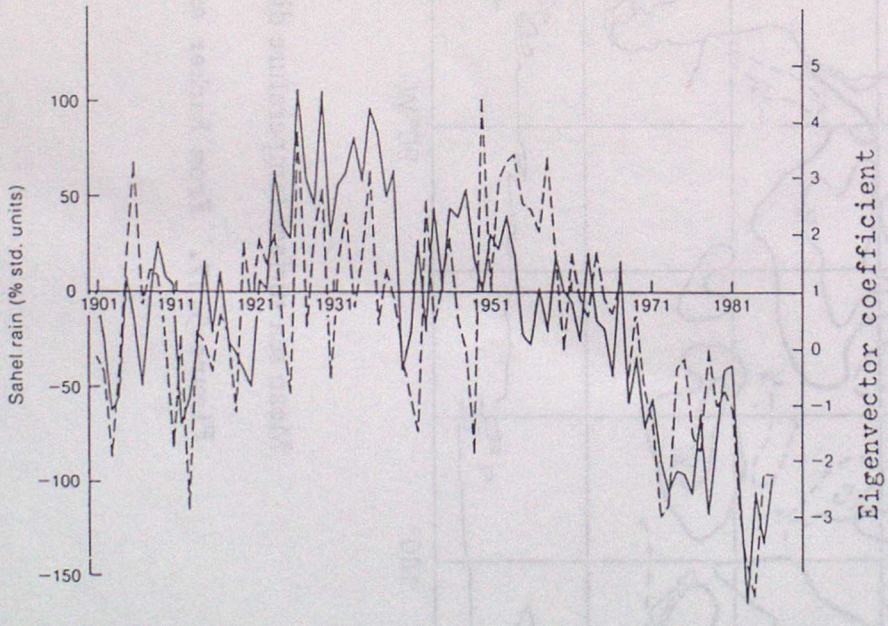

Coefficient of the third all-seasons covariance eigenvector of global SSTA in July to September (solid line) along with Sahel rainfall (dashed line) 1901–86.

Figure 5.19. From Parker et al (1988).

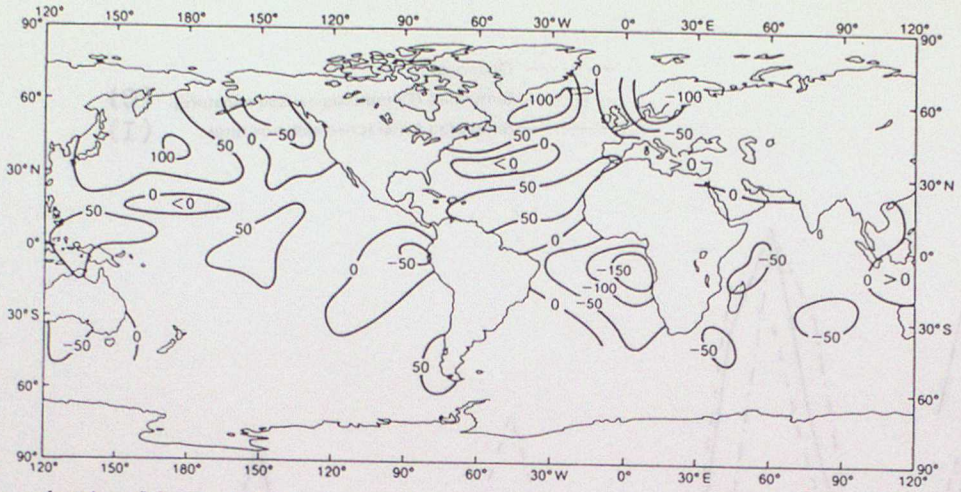

The sixth all-seasons covariance eigenvector of global SSTA, 1901-80. The pattern is scaled so that the sum of squares of 10° latitude x longitude values equals 10^6.

Figure 5.20. From Parker et al (1988).

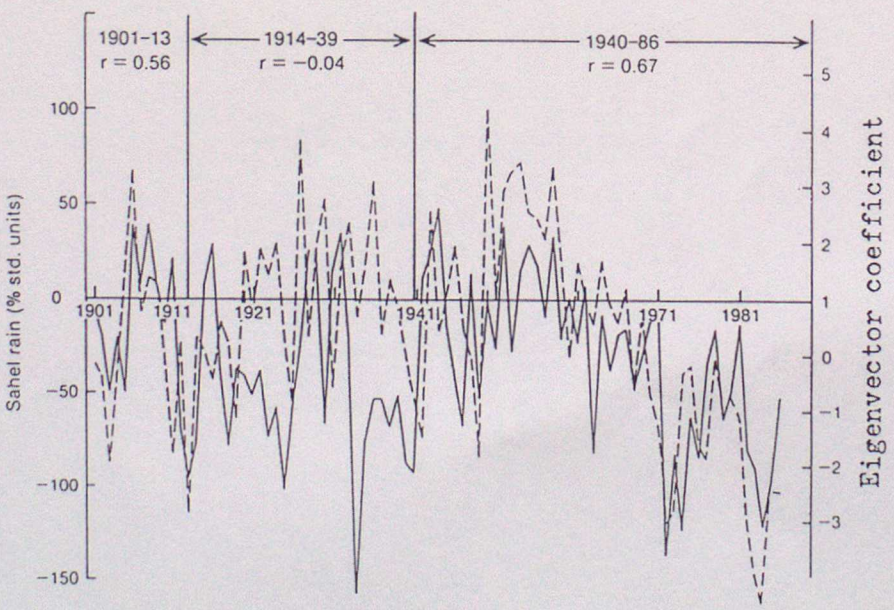

Coefficient of the sixth all-seasons covariance eigenvector of global SSTA in July to September (solid line) along with Sahel rainfall (dashed line) 1901-86.

Figure 5.21. From Parker et al (1988).

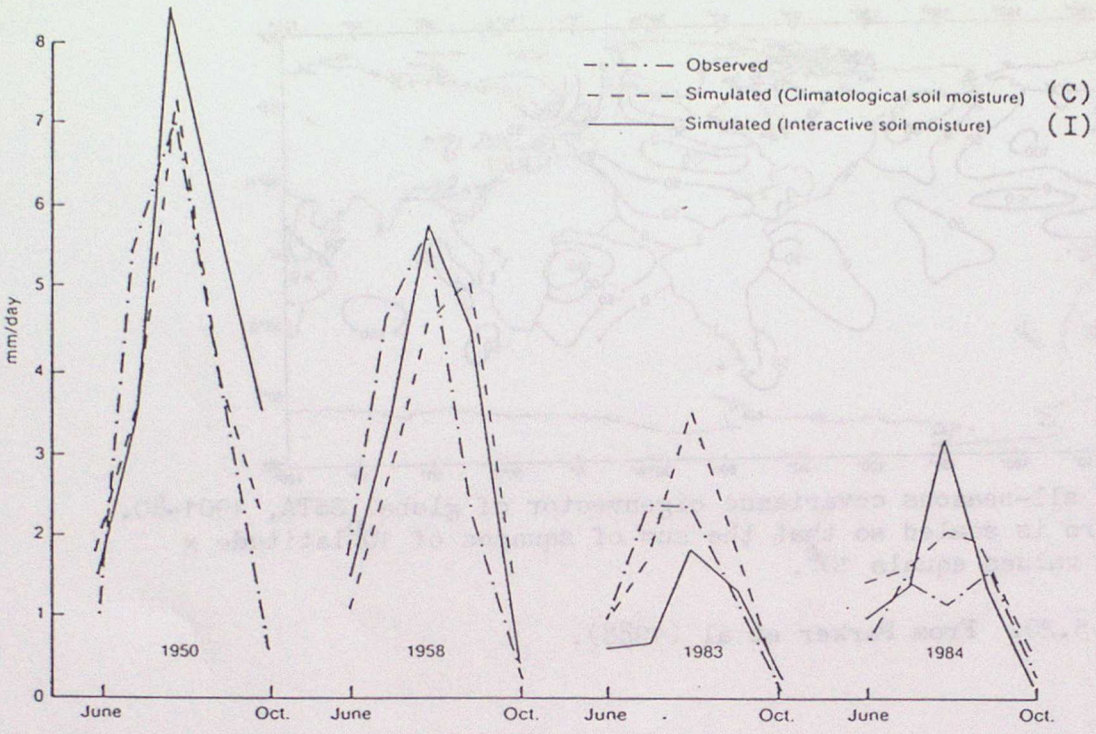

Time series of simulated rainfall for the whole Sahel for experiments 1950(I), 1958(I), 1983(I), 1984(I), 1950(C), 1958(C), 1983(C) and 1984(C), together with the corresponding observed rainfall.

Figure 5.22. From Owen et al (1988).

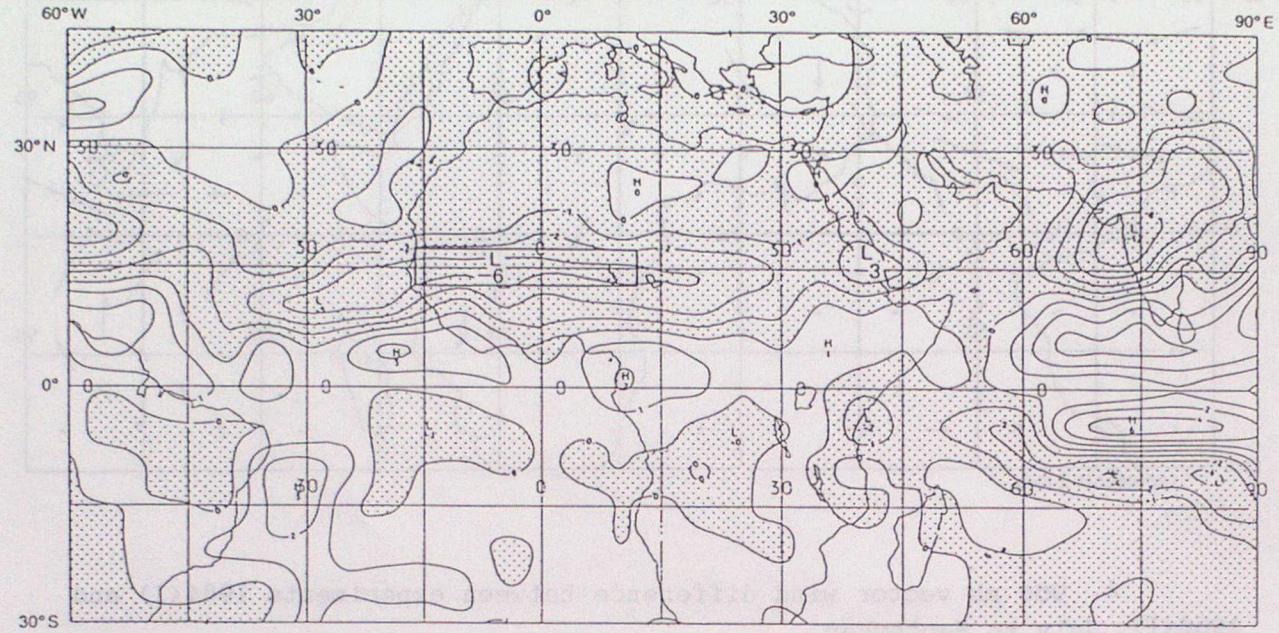

A

Modelled rainfall, difference between experiments 1984(I) and 1950(I) for July to September. Contours are at 0, ±1, 2, 4, 8, and 16 mm day^{-1}, with negative areas stippled.

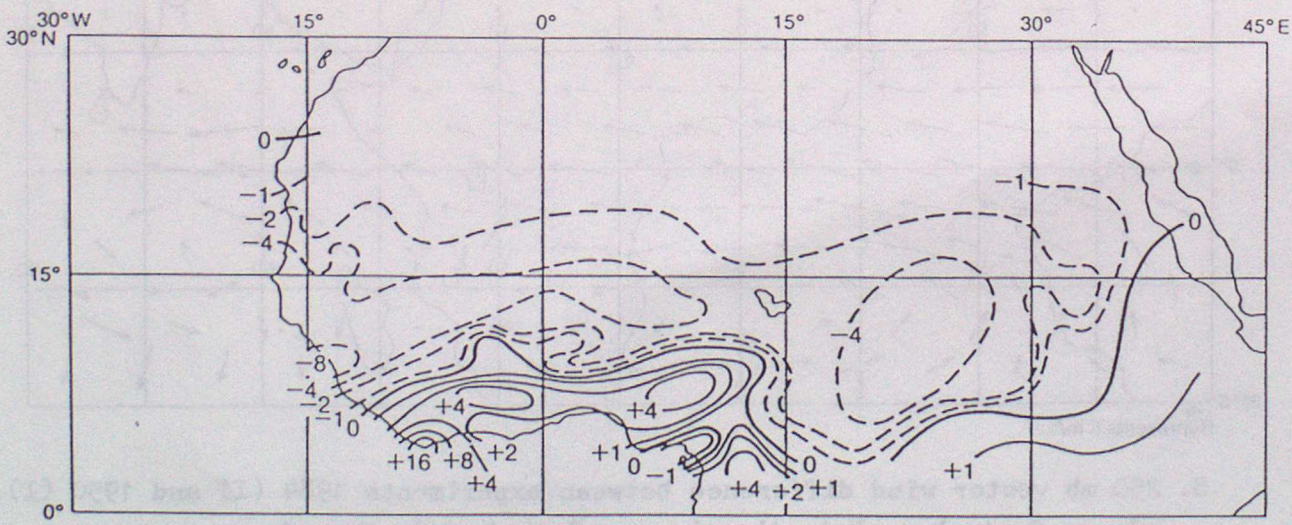

B

Observed rainfall, difference between 1984 and 1950 for July to September. Contours as in A.

Figure 5.23. From Owen et al (1988).

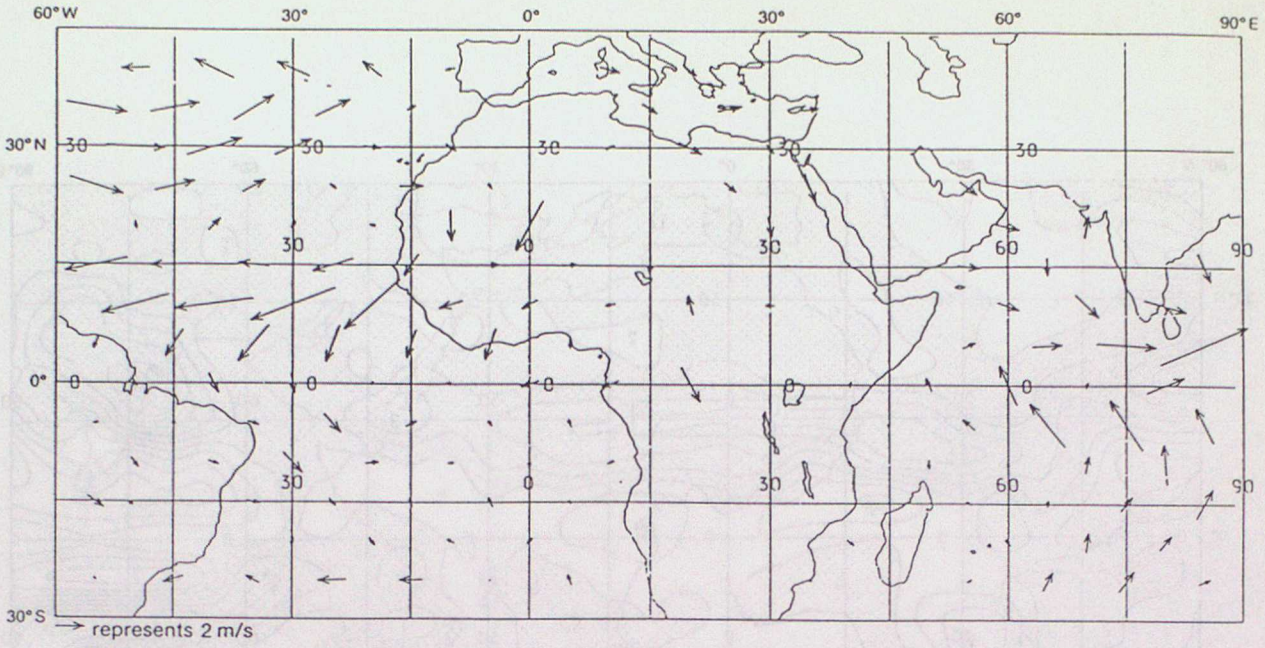

A. 950 mb vector wind difference between experiments 1984(I) and 1950(I). July to September.

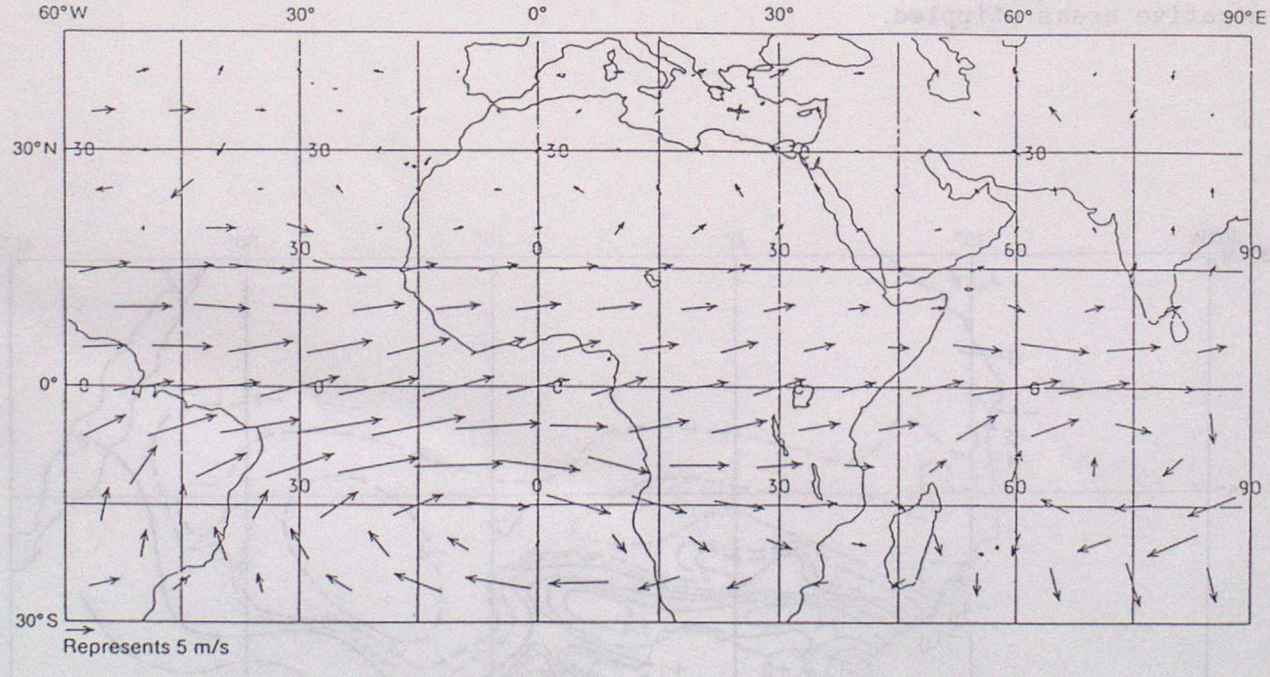

B. 250 mb vector wind difference between experiments 1984 (I) and 1950 (I). July to September. Note the change of wind scale from A.

Figure 5.24. From Owen et al (1988).

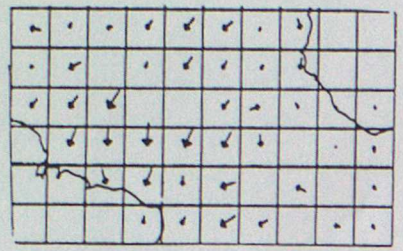

JAN

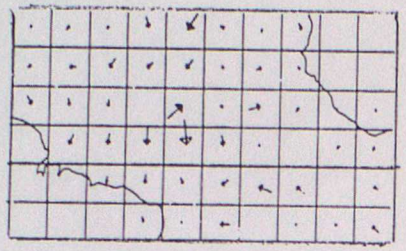

FEB

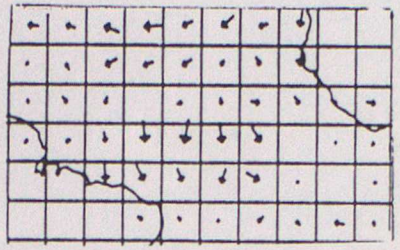

MAR

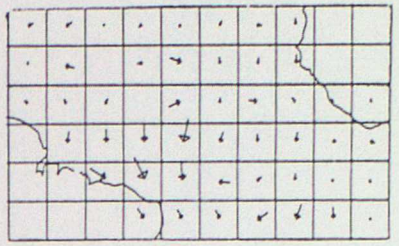

APR

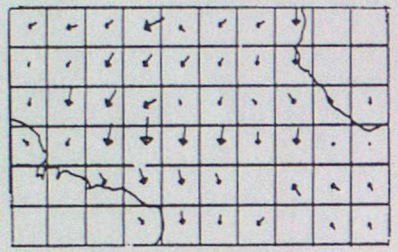

MAY

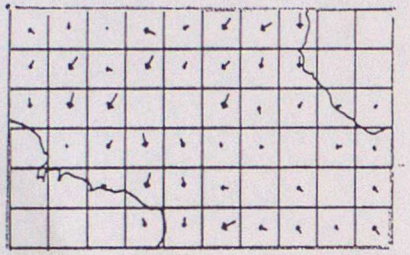

JUNE

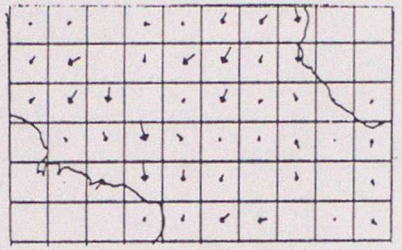

JULY

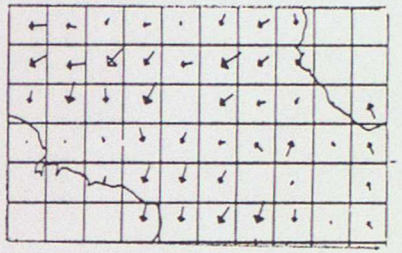

AUG

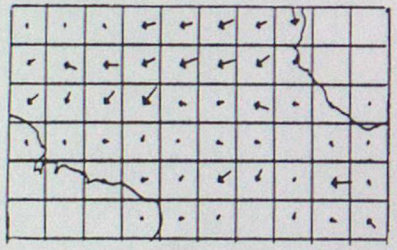

SEPT

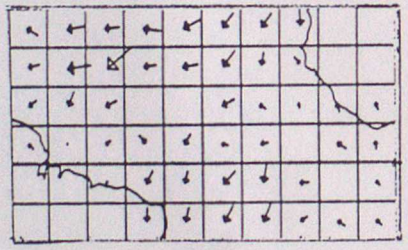

OCT

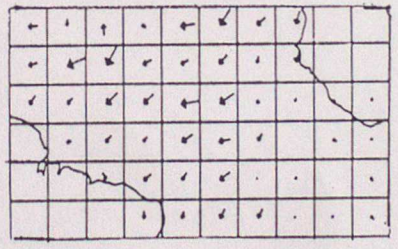

NOV

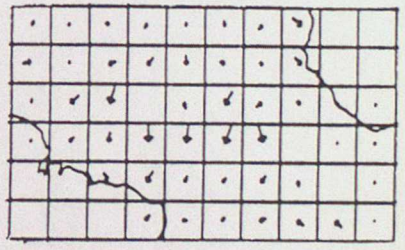

DEC

← REPRESENTS 2 M/SEC

Figure 5.25 Surface winds, 1968-79 relative to 1950-59.
From the Comprehensive Ocean-Atmosphere Data Set (COADS).
(Woodruff et al (1987))

INDEX TO LONG-RANGE FORECASTING AND CLIMATE RESEARCH SERIES

1) THE CLIMATE OF THE WORLD - Introduction and description of world climate.
by C K Folland (March 1986)

2) THE CLIMATE OF THE WORLD - Forcing and feedback processess.
by C K Folland (March 1986)

3) THE CLIMATE OF THE WORLD - El Nino/Southern Oscillation and the Quasi-biennial Oscillation.
by C K Folland (March 1986)

4) THE CLIMATE OF THE WORLD - Climate change: the ancient earth to the 'Little Ice Age'.
by C K Folland

5) THE CLIMATE OF THE WORLD - Climate change: the instumental period.
by C K Folland (March 1986)

6) THE CLIMATE OF THE WORLD - Carbon dioxide and climate (with appendix on simple climate models).
by C K Folland (March 1986)

7a) Sahel rainfall, Northern Hempishere circulation anomalies and worldwide sea temperature changes, (To be published in the Proceedings of the "Pontifical Academy of Sciences Study Week", Vatican, 23-27 September 1986).
by C K Folland, D E Parker, M N Ward and A W Colman (September 1986) (Amended July 1987)

8) Lagged-average forecast experiments with a 5-level general circulation model.
by J M Murphy (March 1986)

9) Statistical Aspects of Ensemble Forecasts.
by J M Murphy (July 1986)

10) The impact of El Nino on an Ensemble of Extended-Range Forecasts. (Submitted to Monthly Weather Review)
by J A Owen and T N Palmer (December 1986)

11) An experimental forecast of the 1987 rainfall in the Northern Nordeste region of Brazil.
by M N Ward, S Brooks and C K Folland (March 1987)

12) The sensitivity of Estimates of Trends of Global and Hemispheric Marine Temperature to Limitations in Geographical Coverage.
by D E Parker (April 1987)

13) General circulation model simulations using cloud distributions from the GAPOD satellite data archive and other sources.
by R Swinbank (May 1987)

14) Similation of the Madden and Julian Oscillation in GCM Experiments.
by R Swinbank (May 1987)

15) Numerical simulation of seasonal Sahel rainfall in four past years using observed sea surface temperatures.
by J A Owen, C K Folland and M Bottomley (April 1988)

16) Not used

17) A note on the use of Voluntary Observing Fleet Data to estimate air-sea fluxes.
by D E Parker (April 1988)

18) Extended-range prediction experiments using an 11-level GCM
by J M Murphy and A Dickinson (April 1988)

19) Numerical models of the Raingauge Exposure problems - field experiments and an improved collector design.
by C K Folland (May 1988)

20) An interim analysis of the leading covariance eigenvectors of worldwide sea surface temperature anomalies for 1901-80.
by C K Folland and A Colman (April 1988)

21) Prospects for long range forecasting for the United Kingdom.
by A Dickinson and C K Folland (July 1988)

22) CLIMATE OF THE WORLD (Restricted Issue) 1. Introduction to world climate
2. Description of world climate
by C K Folland and D E Parker (July 1988)

23) CLIMATE OF THE WORLD (Restricted issue) 3. Climatic forcing and feedback processes. I. Forcing from above.

4. Climatic forcing and feedback processes. II. Interactions with land surface
by C K Folland and D E Parker (July 1988)

24) CLIMATE OF THE WORLD (Restricted Issue) 5. Ocean-atmosphere interaction
by D E Parker and C K Folland (July 1988)

25) CLIMATE OF THE WORLD (Restricted Issue) 6. The El Nino/Southern Oscillation, the Quasi-Biennial Oscillation, and the 30-60 day variations.
by C K Folland and D E Parker (July 1988)

26) CLIMATE OF THE WORLD (Restricted Issue) 7. A review of palaeoclimate from the early Earth to the Pleistocene ice ages

8. Climate from the late glacial to the "Little ice age"
by C K Folland and D E Parker (July 1988)

27) CLIMATE OF THE WORLD 9. Climatic change in the instrumental period
(Restricted Issue) by D E Parker and C K Folland (July 1988)

28) CLIMATE OF THE WORLD 10. Carbon dioxide and other greenhouse gases, and
(Restricted Issue) climatic variation
(with appendix on simple climate models).
by D E Parker, C K Folland and D J Carson
(July 1988)